Study on Composite Electrodes of Oxoacid Cathode Materials with Carbon and their Electrochemical Performance

(オキソ酸塩系正極材料とカーボン材料からなるコンポジット電極およびその電気化学的特性に関する研究)

Dai Okada

Graduate School of Science and Technology,
Niigata University
8050 Ikarashi 2-nocho, Niigata 950-2181
Japan

Preface

The work of this thesis has been carried out under the guidance of Professor Dr. Mineo Sato at Department of Applied Chemistry and Chemical Engineering, Faculty of Engineering, Niigata University.

The object of this thesis is to elucidate the electrochemical characteristics of composite electrodes of oxoacid cathode materials with carbons.

The author wishes that the results obtained in this study provide useful suggestion and information for further development of the electrodes of secondary batteries.

Dai Okada

Graduate School of Science and Technology,
Niigata University
8050 Ikarashi 2-nocho, Niigata 950-2181
Japan

Contents

General introduction

From a perspective of popularization of plug-in hybrid (PHV) and electrical vehicles (EV) that can be one of the most promising way to solve global environmental issues, a demand for the large scale secondary battery is an evitable problem. Iron and vanadium, incorporated in $Na_3V_2(PO_4)_3$, $Li_3V_2(PO_4)_3$ and $LiFePO_4$ which are attractive cathode materials in lithium/sodium ion batteries, are abundant resources on earth. In an actual application, the cathode materials produced at low cost in large scale are desirable for the fabrication of large scale battery. Carbon coating for these oxoacid-based cathode materials that are electronic insulating ionic crystals is known to enhance electrochemical properties due to the enhancement in electronic conductivity of the particle surfaces.

In this study, the author has tried to develop a new synthetic method to produce fine cathode particles on which electronically conductive carbon layers are coated. A conventional solid state synthesis using polystyrene as a carbon source for carbon coating was adopted for the synthesis of the oxoacid cathode materials, $Na_3V_2(PO_4)_3$, $Li_3V_2(PO_4)_3$ and $LiFePO_4$. The resulting cathode materials were nano-sized particles. The carbon coated samples were proved to be much smaller crystal particles than the non-carbon coated materials. The most feature obtained from the method used in this study is the achievement of nano-sized particle synthesis and the improvement of electronic conductivity at the same time. In addition, the method modified by the use of newly developed carbon black particles gave much better performance to the oxoacid cathode materials.

The thesis is comprised from four main chapters as follow：

Chapter one describes the introduction for this work.

Chapter two describes the syntheses of oxoacid-based cathode materials, $Na_3V_2(PO_4)_3$, $Li_3V_2(PO_4)_3$ and $LiFePO_4$.

Chapter three describes the electrochemical performances of the synthesized cathode materials.

The section one of this chapter describes the details of electrochemical properties of carbon coated $Na_3V_2(PO_4)_3$/C composites electrodes synthesized by the solid phase process.

The section two of this chapter describes the details of improvement of high rate performances

for Ti-doped $Li_3V_2(PO_4)_3$ cathode materials.

The section three of this chapter describes the details of electrochemical properties of $LiFePO_4$ cathode materials coated with newly developed carbon black.

Chapter four describes general remarks and conclusions of this thesis.

List of publication

[1] Electrochemical Properties of $LiFePO_4$ Cathode Materials Coated with Newly Developed Carbon Black.

Dai Okada, Takuma Sugiki, Kazuyoshi Uematsu, Atsushi Itadani, Kenji Toda, Mineo Sato, Togo Yamaguchi, Nozomi Arimitsu, and Shogo Nishikawa.

Electrochemistry, **83**(10), 858~860(2015).

[2] Improvement of High Rate Performances for Ti-Doped $Li_3V_2(PO_4)_3$ Cathode Materials.

Dai Okada, Fumiya Nakano, Kazuyoshi Uematsu, Hirokazu Okawa, Atsushi Itadani, Kenji Toda, and Mineo Sato.

Electrochemistry, .**83**(10), 828~830(2015).

1. Introduction

Lithium ion batteries have been widely used for the portable electronic devices because of their high energy density and excellent cycle performance for decades. The typical cathode materials for the lithium ion batteries are basically divided into two categories; one is the lithium transition metal oxides like $LiCoO_2$, $LiNiO_2$ and $LiMn_2O_4$, the other the lithium oxoacid compounds like $LiFePO_4$, Li_2FeSiO_4 and $Li_3V_2(PO_4)_3$. The former materials are semiconductors with relatively high electronic conductivity, while the latter materials are fundamentally insulators which do not work as a cathode material with leaving them as they are.

For practical usage of the oxoacid compounds for the secondary batteries, cathode materials need to be improved on the electronic conductivity of the particle surfaces.[1] For Li ion diffusivity between active material surfaces and electrolyte, electronic conductivity should be enhanced. So many studies have been done to improve the active material surface conductivity coated by carbons or electronically-conductive metals. However, in order to making Li ions diffusive around liquid-solid phase boundaries, the coating materials should not cover the whole of the particle surface at all.[2-5] Therefore, the coating materials are preferable to contain appropriate amount of voids for farther Li diffusion around the boundaries. At viewpoint of making the surface Li-ion-diffusive and electronically conductive simultaneously, a carbon coating method is a realistic and reasonable way.

For enhancement in Li ion diffusivity inside a crystal, microparticulation of active materials is one of the most effective ways for reduction in Li diffusion path. Many studies have been done to obtain fine particles with superior ion diffusivity.[3–5] Carbon coating for oxoacid-based cathode materials that are electronic insulating ionic crystals is known to enhance electrochemical properties due to enhancement in electronic conductivity on particle surface. In a preliminary study by our group, it has been proved that nano-cathode materials like $LiFePO_4$ or $Li_3V_2(PO_4)_3$ can be synthesized by a conventional solid state synthesis using polystyrene as a carbon source. Compared to non-carbon coated materials, the materials synthesized by this method are composed of much smaller sized nano particles. From the results in the variation of calcination temperature for graphitization, it has been concluded that the

deposited carbons behave as the obstacles to prevent particle growth. For simultaneous achievements of nano-paticulation and improvement of surface electronic conductivity in cathode materials at the same time, this method is quite actual and reasonable.

From a perspective of popularization of plug-in hybrid (PHV) and electrical vehicles (EV) that can be one of the most promising way to solve global environmental issues, a demand for the large scale secondary battery is an evitable problem. Iron and vanadium, incorporated in $Na_3V_2(PO_4)_3$, $Li_3V_2(PO_4)_3$ and $LiFePO_4$ which are attractive cathode materials in lithium/sodium ion batteries, are abundant resources on earth. At the viewpoint of resource availability, it is clear that elemental sodium is more abundant than lithium on earth.

In this study, the author have tried to develop a new synthetic method to produce fine cathode particles on which electronic conductive carbon layers are coated. The conventional solid state synthesis using polystyrene as a carbon source was adopted for synthesis of the oxoacid cathode materials, $Na_3V_2(PO_4)_3$, $Li_3V_2(PO_4)_3$ and $LiFePO_4$ The resulting cathode materials were nano-sized particles. The carbon coated samples was proved to be much smaller crystal particles than the non-carbon coated materials. The most feature obtained from the method used in this study is the achievement of nano-sized particle synthesis and the improvement of electronic conductivity at the same time. In addition, the method modified by the use of newly developed carbon black particles gave much better performance to the oxoacid cathode materials. The thesis is comprised from three main themes; the first describes electrochemical properties of carbon coated $Na_3V_2(PO_4)_3$/C composites electrodes synthesized by the solid phase process, the second improvement of high rate performances for Ti-doped $Li_3V_2(PO_4)_3$ cathode materials, and the third electrochemical properties of $LiFePO_4$ cathode materials coated with newly developed carbon black.

The first theme:

So far, the oxoacid cathode materials like NASICON compound $Na_3V_2(PO_4)_3$ and NASICON-related compound $Li_3V_2(PO_4)_3$ have been studied on the crystallographic features and the electrochemical properties.[6–19] NASICON materials have three-dimensional polyanionic structures built up with XO_4 tetrahedra (X = W, P, S, Si, Mo) sharing corners with MO_6 octahedra (M = Fe, Ti, Sc, Hf, V, Ti, Zr), which make up the framework anion

$(M_2(XO_4)_3)^{3-}$. The two independent alkali cation sites are presented in the framework and partially occupied in the channels with two different oxygen environments. One site is a six-fold coordination M(1) site, the other is an eightfold coordination M(2) site. The open structure of $M_2(PO_4)_3$ constitutes fast alkali ionic conduction[6]. Consequently, possible oxygen liberation from the structure which is sometimes encountered in other simple oxide cathode materials become suppressed.[12–14] The rhombohedral phase of $Na_3V_2(PO_4)_3$, one of the typical NASICON type compounds, originally have been investigated mainly for their properties of fast ionic conduction as a solid electrolyte. Moreover, $Na_3V_2(PO_4)_3$ is expected as a promising candidate for sodium-ion battery electrodes to meet increasing demands for large scale and high power performance batteries. $Na_3V_2(PO_4)_3$ has two different voltage plateaus at around 3.3 V and 1.6 V, based on the V^{4+}/V^{3+} and V^{3+}/V^{2+} redox couples, respectively. The theoretical discharge capacity of $Na_3V_2(PO_4)_3$ is 118 mAh g^{-1} at around 3.3 V with two Na ions being extracted. The phosphate cathodes display excellent electrochemical and thermal stability due to the stronger phosphorous-metal bonds, compared to lithium metal oxides. Hence, this study has focused on the $Na_3V_2(PO_4)_3$ oxoacid cathode materials for sodium ion secondary batteries. However, the electrical conductivity of $Na_3V_2(PO_4)_3$ is as low as $LiFePO_4$ (~10^{-9} S/cm), which limits its electrochemical performance.[20] To solve this problem, the carbon coating for active materials is commonly performed by many researchers.[20,21] So, the author has adapted the two step calcination method applied to carbon coated $LiFePO_4$ active cathodes which was invented by our group. This method uses polystyrene as a carbon source which is added to thermally decomposed raw materials of $LiFePO_4$. Then, the materials are mixed and calcined at high temperatures. The obtained carbon coated $LiFePO_4$ could achieve desirable battery performance for a practical usage. Therefore, the carbon coated $Na_3V_2(PO_4)_3$ ($Na_3V_2(PO_4)_3$/C) was synthesized by the two step synthesis method to confirm the effectiveness of the carbon coating process for other oxoacid cathode materials. Moreover, the morphology and electrochemical properties of obtained $Na_3V_2(PO_4)_3$/C were investigated.

The second theme:

Lithium vanadium(III) phosphate, $Li_3V_2(PO_4)_3$, has three independent lithium sites in the low-temperature form, where all the three type lithium ions located on these sites can take part

in redox reaction.[12,22] Therefore, this material is capable to keep a large theoretical capacity of 197 $mAhg^{-1}$ and high redox voltages during all three lithium ions delivery.[3] This potential performance is desirable for practical use to achieve high energy density. However, it is difficult to bring out the proper performance of $Li_3V_2(PO_4)_3$ because of its low electronic conductivity with the order of 10^{-7} Scm^{-1}.[23,24] Our group has so far investigated crystal structure and ionic conductivity of the $Li_{3-2x}(V_{1-x}Zr_x)_2(PO_4)_3$ materials ($0 \leq x \leq 0.2$) prepared by a solid state reaction, confirming that monoclinic $Li_3V_2(PO_4)_3$ was s stabilized by substituting Zr for V sites in $Li_3V_2(PO_4)_3$, normally the structure being changed from α-phase to β-phase at about 120°C and from β-phase to γ-phase at about 180°C.[25] Furthermore, the $Li_{3-2x}(V_{1-x}Zr_x)_2(PO_4)_3$ materials have been reported to exhibit a high charge-discharge performance.[5] Such electrochemical performances suggest that Li ionic conductivity is improved by substituting Zr for V sites in $Li_3V_2(PO_4)_3$ and also that the phase transition from α- to γ-phase results in increase in the Li ion mobility. In the previous work on electrochemical performance, the electrochemical properties of $Li_3V_2(PO_4)_3$ where the V sites were substituted by other transition metals were investigated in detail.[19] Titanium as a substitution element has been known to be one of the promising elements as an additive stuff for the improvement of electrical conductivity (especially ionic conductivity) of $Li_3V_2(PO_4)_3$.[25–27] However, such cathode materials were not electronically modified by carbon coating, giving relatively poor electrochemical performances. In this work, the Ti-doped $Li_3V_2(PO_4)_3$ cathode materials were prepared by calcining with polystyrene so as to coat carbon layers on the surface of the products, and their electrochemical performance was carefully investigated concerned with the impact of carbon coated Ti-doped $Li_3V_2(PO_4)_3$ with the high temperature γ-phase which has high ionic conductivity.

The third theme:

The group to which the author belongs have studied carbon coating effects on electrochemical properties of $LiFePO_4$ which were synthesized by hydrothermal/solvothermal method,[28] micro wave synthesis method[29,30] and solid state synthesis.[31] These carbon coated samples could achieve excellent durable cycle performance and superior rate performance. In particular, the solid state synthesis using polystyrene is one of the most promising ways to obtain carbon-coated $LiFePO_4$ ($LiFePO_4$/C) with excellent electrochemical performance. In this method,

polystyrene as a carbon source is added to thermally decomposed raw materials for $LiFePO_4$. Then, these materials are mixed and calcined at high temperatures. The obtained $LiFePO_4$/C is composed of fine particles on which uniform carbon layers are coated, providing good battery properties. Generally, carbon black is used to enforce electronic conductivity in the electrode. The primary particles of carbon black are quite small compared to particles of cathode materials. Also the primary particles of carbon black form continuous linking structures ("structure") and develop their "structure". Therefore, carbon black can adhere to the active material particles and make contacts among active materials. Additionally, control of primary particle size and "structure" features is equal to dominate the dispersion state of carbon black. Recently, a new type of carbon black focused on the use in lithium ion batteries, labeled as "CB1", has been developed by Asahi Carbon Co. Ltd., Japan. CB1 consists of the smaller sized primary particles with a diameter of 10 nm and has a relatively large specific surface area of 336 $m^2\ g^{-1}$ (DBP absorption number: 206 ml $(100\ g)^{-1}$), in comparison with the commercially available acetylene black (primary particle size: 35 nm; surface area: 68 $m^2\ g^{-1}$; DBP absorption number: 175 ml $(100\ g)^{-1}$). As is often the case with a large number of active materials in lithium ion batteries, electronic conductivity is not enough even in oxide active materials. In usual, to keep the electrically good contact between electrode materials, the carbon black has generally been used as a conduction supporting agent in electrodes. Furthermore, as a strategy to provide more efficient electronic conductivity toward the active materials and reduce particle size of active materials, the carbon coating on the surface of active materials has been accepted to be useful and realistic technologies.[32–38] In this study, focusing on the property of CB1 which has the smaller primary particle size and developed "structures", the author has investigated the potential of CB1 that rolls up the active material particles and works like carbon layers derived from polymer materials.

2. Experimental

2.1. Preparation and Characterization of $Na_3V_2(PO_4)_3$

$Na_3V_2(PO_4)_3$ samples were prepared as follows. Stoichiometric amounts of Na_2CO_3, NH_4VO_3 and $NH_4H_2PO_4$ were mixed by ball-milling with toluene as a mixing solvent for 4 h. The mixture was heated at 300°C for 4 h in an Ar atmosphere in a tubular furnace and then cooled to room temperature. The $Na_3V_2(PO_4)_3$ precursors prepared were reground by ball-milling for 2 h, followed by heating at 600, 700, 800 and 900°C for 12 h in an Ar + 5 % H_2 atmosphere in the tubular furnace to obtain the $Na_3V_2(PO_4)_3$ samples without carbon-coating. After heating the mixture of the starting materials at 300°C as described above, the $Na_3V_2(PO_4)_3$ precursors obtained were mixed with polystyrene by the ball mill with toluene as a mixing solvent for 2 h and then calcined at 600, 700, 800 and 900°C for 12 h in an Ar + 5 % H_2 atmosphere in the tubular furnace to prepare the carbon-coated $Na_3V_2(PO_4)_3$/C samples.

Thermogravimetric-differential thermal analysis (TG-DTA) was conducted on a TG-DTA6300 EXSTAR6000 (Seiko Instruments Inc.) in the temperature range from 10 to 950°C under an Ar atmosphere. Powder X-ray diffraction (XRD) profiles were collected in the range from 10 to 90° using an MX-Labo diffractometer (MAC Science Co. Ltd.) with monochromatic Cu*K*α radiation (λ = 0.154056 nm) under 25 mA and 40 kV at room temperature. Rietveld refinement was performed using RietanFP software[29] for analyzing XRD patterns. Scanning electron microscopy (SEM) measurements were carried out on a JSM-5800 (JEOL Co. Ltd.). Transmission electron microscopy (TEM) images for the carbon-coated $Na_3V_2(PO_4)_3$ samples were taken using a JEM-2800F (JEOL Co. Ltd.). Specific surface area measurements were conducted on a Flowsob Ⅱ 2300 (Shimadzu Co. Ltd.). Raman spectra were recorded by a HORIBA JOBIN YVON Lab RAM HR (HORIBA, Ltd.) operating at a resolution of 1 cm^{-1}.

A cathode was prepared by mixing 85 wt% active material $Li_{3-2x}(V_{1-x}Ti_x)_2(PO_4)_3$, 8 wt% acetylene black, and 7 wt% polyvinylidene difluoride (PVDF) in an *N*-methyl-2-pyrrolidone (NMP) solvent. The electrochemical measurements were performed using a two electrode cell, namely, a sodium metal anode and 1 M $NaPF_6$ solved in a propylene carbonate : dimethyl carbonate (1:1 v/v) solution as a counter electrode and electrolyte, respectively. The

galvanostatic charge-discharge cycle measurements at room temperature were carried out at various rates with a cut off voltage range of 2.0 to 4.0 V versus Na/Na^+ using a PFX2011S charge-discharge unit (Kikusui Electronics Co., Japan).

2.2 Preparation and Characterization of Ti-doped $Li_{3-2x}(V_{1-x}Ti_x)_2(PO_4)_3$

$Li_{3-2x}(V_{1-x}Ti_x)_2(PO_4)_3$ (x = 0, 0.025, 0.050, 0.10, 0.20) samples were prepared as follows. Stoichiometric amounts of Li_2CO_3, V_2O_5, $NH_4H_2PO_4$, and TiO_2 were mixed by ball-milling with toluene as a mixing solvent for 4 h. The mixture was heated at 300°C for 6 h in an Ar atmosphere in a tubular furnace and then cooled to room temperature. The $Li_{3-2x}(V_{1-x}Ti_x)_2(PO_4)_3$ precursors prepared were reground by ball-milling for 2 h, followed by heating at 880°C for 12 h in an Ar + 5 % H_2 atmosphere in the tubular furnace to obtain the $Li_{3-2x}(V_{1-x}Ti_x)_2(PO_4)_3$ samples without carbon-coating. After heating the mixture of the starting materials at 300°C as described above, the $Li_{3-2x}(V_{1-x}Ti_x)_2(PO_4)_3$ precursors obtained were mixed with polystyrene by the ball mill with toluene as a mixing solvent for 2 h and then calcined at 880°C for 12 h in an Ar + 5 % H_2 atmosphere in the tubular furnace to prepare the carbon-coated $Li_{3-2x}(V_{1-x}Ti_x)_2(PO_4)_3$/C samples.

Diffraction scanning calorimetry (DSC) measurements were conducted on a Thermo plus EVO2 DSC 8231 (Rigaku Co.) in the temperature range from 10 to 300°C under an Ar atmosphere. Powder X-ray diffraction (XRD) profiles were collected in the range from 10 to 90° using an MX-Labo diffractometer (MAC Science Co. Ltd.) with monochromatic Cu$K\alpha$ radiation (λ = 0.154056 nm) under 25 mA and 40 kV at room temperature.

A cathode was prepared by mixing 85 wt% active material $Li_{3-2x}(V_{1-x}Ti_x)_2(PO_4)_3$, 8 wt% acetylene black, and 7 wt% polyvinylidene difluoride (PVDF) in a *N*-methyl-2-pyrrolidone (NMP) solvent. The electrochemical measurements were performed using a two electrode cell, namely, a lithium metal anode and 1 M $LiPF_6$ solved in an ethylene carbonate : dimethyl carbonate (1:1 v/v) solution as a counter electrode and electrolyte, respectively. The galvanostatic charge-discharge cycle measurements at room temperature were carried out at various rates with a cut off voltage range of 2.0 to 4.8 V versus Li/Li^+ using a PFX2011S charge-

discharge unit (Kikusui Electronics Co., Japan).

Non carbon-coated specimens for the conductivity measurements were prepared by pressing the powder sample into a disk. The disk was sintered at 930°C for 10 h under an Ar atmosphere. The two opposite sides of the disk were coated with a silver paste. An LCR meter (NF Co., ZM2375) was used for impedance measurements in the temperature range from 20 to 200°C under an Ar atmosphere. The conductivity was determined by the complex impedance diagrams obtained using alternating currents with frequencies between 0.02 and 5.5 MHz.

2.3 Preparation and Characterization of $LiFePO_4$

The carbon-coated $LiFePO_4$ samples were synthesized by a solid state reaction with CB1, AB and PS as carbon sources. First of all, to synthesize $LiFePO_4$ precursor, stoichiometric amounts of Li_2CO_3, $FeC_2O_4 \cdot 2H_2O$, and $NH_4H_2PO_4$ were mixed by ball-milling with toluene as a mixing solvent for 3 h. The mixture was heated at 320ºC for 5 h in an Ar + 5% H_2 atmosphere in a tubular furnace. In consideration for both mass reduction of the precursor during calcination and deposition of appropriate amount of carbon on particle surfaces, 5 wt% amounts of CB1 and AB relative to the weight of the $LiFePO_4$ precursor were added to obtain the materials containing about 6 ~ 8 wt% carbon. Also, PS was added 20 wt% relative to the precursor to provide a certain level of uniform carbon-coating on particle surfaces. Similarly, for the sample with CB1 and PS, first, CB1 was added to $LiFePO_4$ precursor, and then PS was added as mentioned above, respectively. The precursors were then mixed with the carbon sources using the ball mill under a dry condition (CB1 and AB) or with toluene as a solvent (PS) for 2 h. After mixing the precursors with CB1, the obtained mixture was further mixed with PS. Finally, these mixtures of the precursors and the carbon sources were heated at 700ºC for 10 h in an Ar atmosphere to obtain four kinds of the carbon-coated $LiFePO_4$ samples (three kinds of $LiFePO_4$ samples carbon-coated with CB1, AB, and PS, respectively, and the $LiFePO_4$ sample carbon-coated with CB1 and PS).

Powder X-ray diffraction (XRD) profiles were collected using an MX-Labo diffractometer (MAC Science Co. Ltd.) with monochromatic Cu$K\alpha$ radiation (λ = 0.154056 nm) under 25 mA

and 40 kV. The elemental analysis of the carbon-coated $LiFePO_4$ samples were performed with a CHN corder (Micro corder JM10, J-Science Lab Co., Ltd.). Scanning electron microscopy (SEM) measurements for cathode electrodes were carried out on a MERLIN VP Compact (Carl Zeiss Microscopy Co. Ltd.). Transmission electron microscopy (TEM) images for the carbon-coated $LiFePO_4$ samples were taken using a Tecnai G^2 20ST (FEI Company).

To clarify the electrochemical properties of carbon-coated $LiFePO_4$ samples, the $LiFePO_4$ cathode was prepared by the slurry-coating technique by mixing 85 wt% active material carbon-coated $LiFePO_4$ (assuming to contain about 6 wt% carbon at electrode in the cases of samples with CB1, AB, and CB1 and PS, and about 2 wt% carbon in the sample with PS), 8 wt% acetylene black, and 7 wt% polyvinylidene difluoride (PVDF) in *N*-methyl-2-pyrrolidone (NMP) solvent. The slurry obtained was coated onto an aluminum foil. A lithium metal foil and 1 M $LiPF_6$ solved in an ethylene carbonate : dimethyl carbonate (1:1 v/v) solution were used as a counter electrode and electrolyte, respectively. The galvanostatic charge-discharge cycles at room temperature were carried out at various rates with a cut off voltage range of 2.0 to 4.0 V versus Li/Li^+ using a PFX2011S charge-discharge unit (Kikusui Electronics Co., Japan).

3. Results and discussion

3.1. Electrochemical Properties of $Na_3V_2(PO_4)_3$/C Composites Synthesized by Solid Phase Process

The thermogravimetric-differential thermal analysis (TG-DTA) measurements were conducted to determine appropriate temperature for the synthesis of the samples of $Na_3V_2(PO_4)_3$ (NVP) and carbon coated $Na_3V_2(PO_4)_3$ (NVP/C). Figure 1 shows the TG-DTA curves of the mixture of raw materials used in the synthesis of NVP. As can be seen from the TG curves, a marked weight loss was confirmed in the temperature range from room temperature to 300˚C. Apparently in the DTA curve, the exothermic reactions occur at around 170 and 190˚C, which correspond to the pyrolytic decomposition of raw materials of NVP, whereas an endothermic reaction occurs at around 280˚C. Taking into account the results, the temperature of 300˚C was adopted as decomposition temperature for the mixture of raw materials used in the synthesis of NVP as described in the experimental session. Looking at the higher temperature region, on the other hand, the DTA curve shows the endothermic and exothermic reactions in the temperature range from 400 to 580˚C. This is probably because the formation reaction of NVP accompanied with a kind of sublimation reaction. Therefore, for both NVP and NVP/C, the main calcination temperatures for the decomposed samples were varied in range of 600-900˚C to evaluate a suitable synthesis temperature Hereafter, the samples obtained are abbreviated as *T*-NVP and *T*-NVP/C (*T*: calcination temperature).

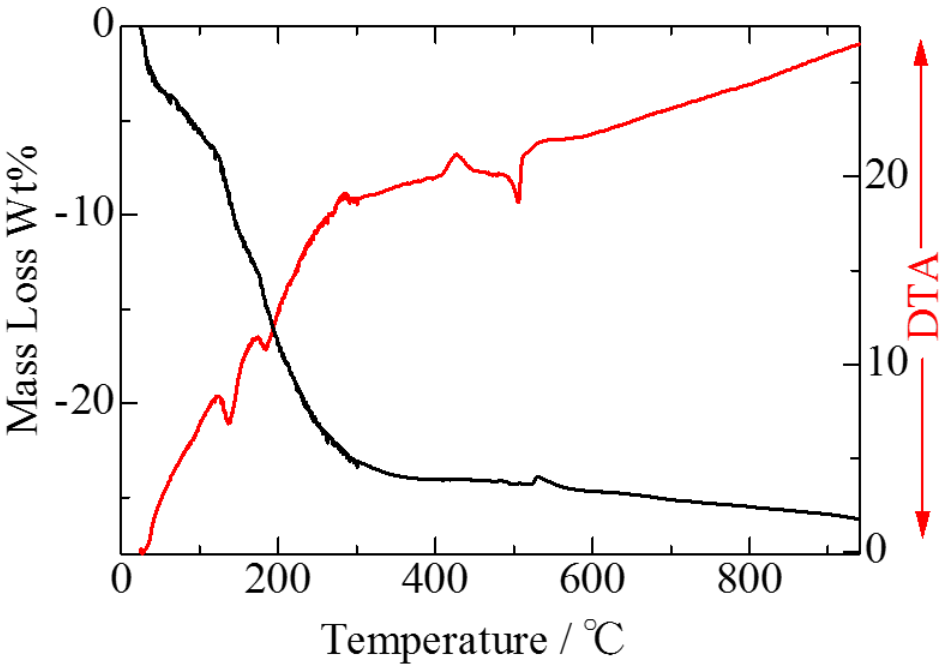

Figure 1. TG-DTA curves of raw materials of $Na_3V_2(PO_4)_3$ in Ar atmosphere from room temperature to 950ºC.

Figure 2 shows the XRD patterns of NVP and NVP/C calcined at various temperatures. Referring to ICSD, the main phase for each sample was identified as NVP with an ordered NASICON structure indexed to rhombohedral. In the cases of the non carbon-coated NVP samples (Figure 2a), an impurity phase is observed at around $2\theta = 30^{\circ}$. In contrast to this, in the carbon-coated NVP/C samples such a phase is hardly seen (Figure 2b). The XRD pattern of the NVP precursor calcined temporarily at 300°C is represented in Figure 2c. For the presented NVP samples, the peak observed at around $2\theta = 30^{\circ}$ (i.e., the impurity phase) is also seen clearly, identified as $NaVP_2O_7$ (ICSD #65696); the peak at $2\theta = 30^{\circ}$ is considered to be due to an intermediate product of $NaVP_2O_7$ for NVP.[20]

The Rietveld refinement was performed using the XRD patterns, and the resultant data are listed at Table 1. For NVP, the ratio of the impurity phase of $NaVP_2O_7$ to $Na_3V_2(PO_4)_3$ ($NaVP_2O_7$: $Na_3V_2(PO_4)_3$) in the samples obtained is found to be larger than that for NVP/C. Such difference observed between NVP and NVP/C can be considered to be responsible for the use of polystyrene as a carbon source. Furthermore, in both cases of 700-NVP and 700-NVP/C, the ratio of the impurity phase of $NaVP_2O_7$ to $Na_3V_2(PO_4)_3$ in the samples is the least among the sample calcined at other temperatures.

The crystalline sizes of the NVP/C samples are apparently smaller than those of the NVP samples. For NVP, furthermore, their crystalline size increases with the increase in the calcination temperature although for NVP/C the crystalline size hardly changes. The detailed discussion is described later, together with other results. Compared with carbon coated NVP/C, the crystalline sizes of NVP were much larger, especially the sample calcined at higher temperatures. There is a tendency that the crystal growth of NVP/C is hardly taken place at any calcine temperatures, though the crystal growth of NVP is apparently taken place as the calcine temperature increases.

(a)

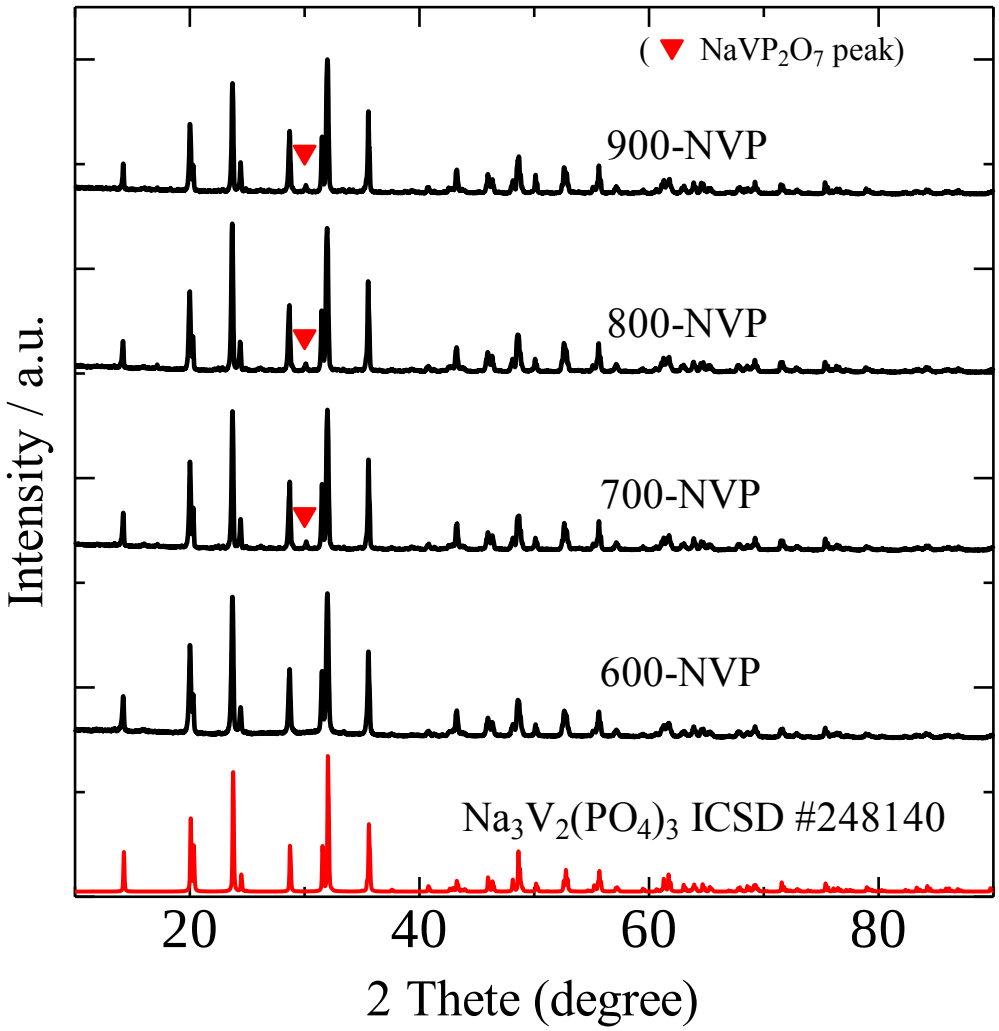
(▼ NaVP2O7 peak)
900-NVP
800-NVP
700-NVP
600-NVP
Na3V2(PO4)3 ICSD #248140
Intensity / a.u.
20
40
60
80
2 Thete (degree)

(b)

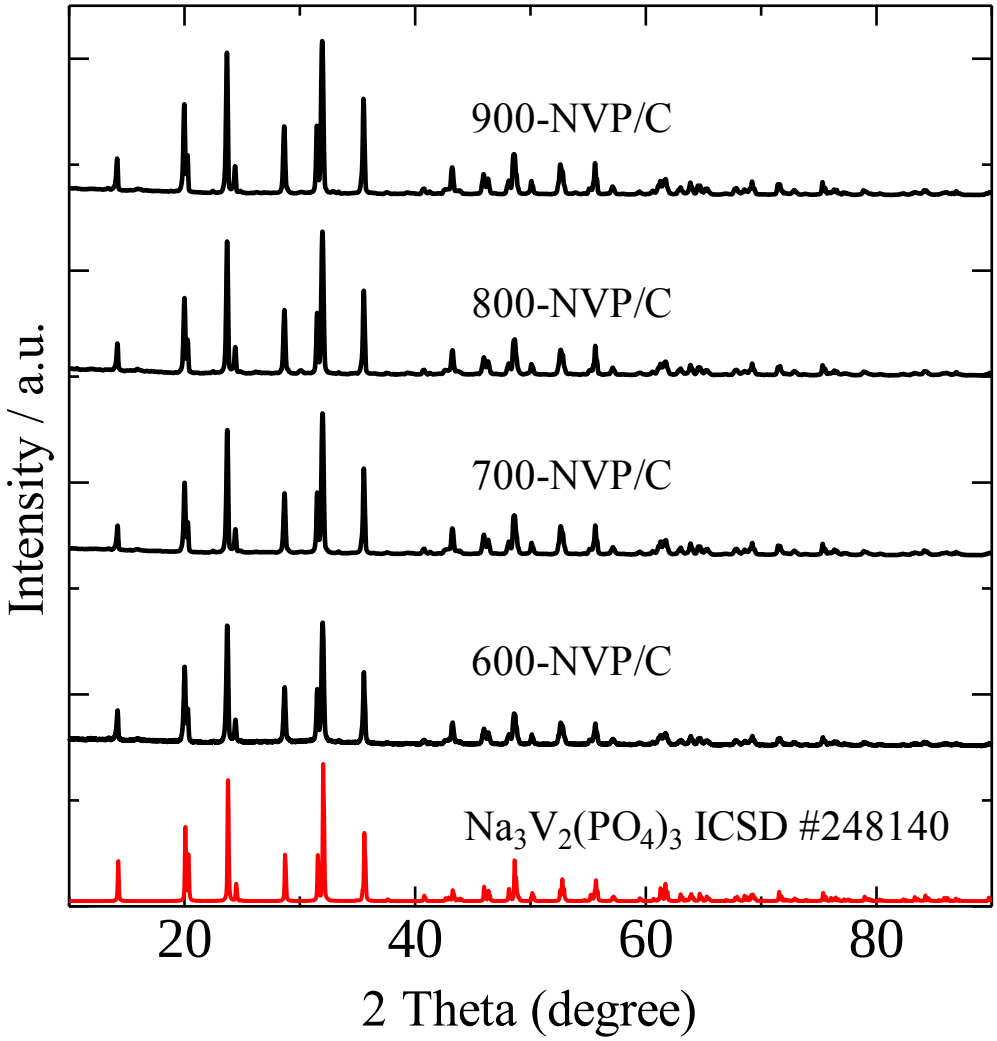
900-NVP/C
800-NVP/C
700-NVP/C
600-NVP/C
Na3V2(PO4)3 ICSD #248140
Intensity / a.u.
20
40
60
80
2 Theta (degree)

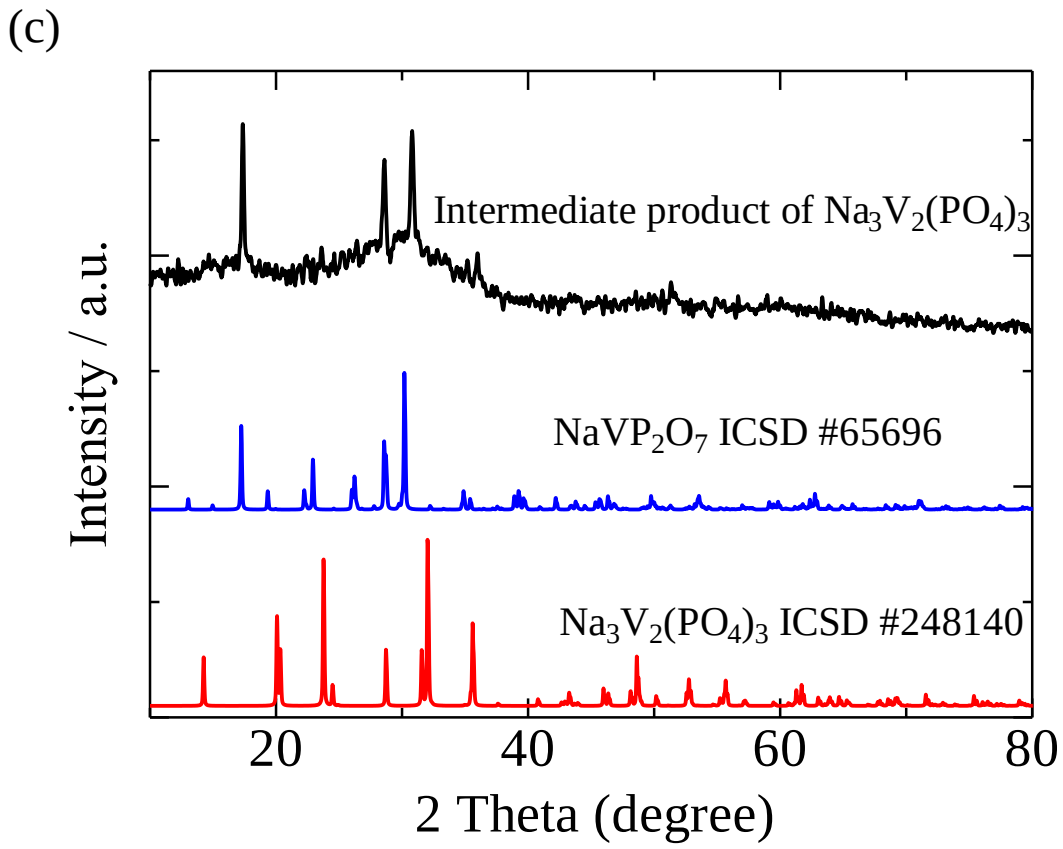

Figure 2. XRD patterns of (a) $Na_3V_2(PO_4)_3$ synthesized without polystyrene at calcine temperatures at 600-900ºC, (b) $Na_3V_2(PO_4)_3$/C synthesized with polystyrene as carbon source at calcine temperatures at 600-900ºC and (c) intermediate product of $Na_3V_2(PO_4)_3$ calcined at 300ºC.

Table 1. Mass ratio of impurity phase of $NaVP_2O_7$ to $Na_3V_2(PO_4)_3$ and crystalline size of (a) $Na_3V_2(PO_4)_3$ synthesized without polystyrene at calcine temperatures above 600ºC (here 600-900ºC) and (b) $Na_3V_2(PO_4)_3$/C synthesized with polystyrene at calcine temperatures above 600ºC (here 600-900ºC). The date were estimated from the calculation results of Rietveld refinements.

(a)

Sample	$Na_3V_2(PO_4)_3$: $NaVP_2O_7$	Crystalline size / nm
600-LVP	83 : 17	164
700-LVP	86 : 14	242
800-LVP	82 : 18	546
900-LVP	85 : 15	591

(b)

Sample	$Na_3V_2(PO_4)_3$: $NaVP_2O_7$	Crystalline size / nm
600-LVP/C	95 : 5	122
700-LVP/C	98 : 2	122
800-LVP/C	92 : 8	132
900-LVP/C	91 : 9	129

Figure 3 shows SEM images of the NVP precursor, NVP/C and NVP. The NVP/C samples were synthesized with polystyrene to coat carbon layers on particle surfaces, and the NVP samples were synthesized without carbon sources under various calcination temperatures. The morphology of intermediate materials of NVP calcined at 300ºC is shown in Figure 3a. There is a trace of melting of raw materials and a number of voids. Compared with the NVP precursor, in Figure 3b, 600-NVP/C exhibits microparticulated morphology by planetary boll milling, but some particles agglutinate as secondary particles. In Figure 3c, the morphology of 700-NVP/C is shown with fine particles given by planetary boll milling and slight particle growth due to the high temperature calcination. This phenomenon is presumed to be promoted with a rise in temperature. In Figures 3d and 3e, 800-NVP/C and 900-NVP/C are shown also with slight particle growth. In the case mixing polystyrene with the NVP precursor, generated carbons would prevent particle growth of NVP even at high calcination temperatures.

Furthermore, to confirm the effects of polystyrene on prevention of particle growth, 700-NVP and 800-NVP were synthesized without carbon source. Figure 3f shows the SEM images of 700-NVP particles, showing the observed particle sizes to be about 1.0-4.0 μm. The particles of 700-NVP indicate a sign of slight crystal growth by 700ºC heating. With comparison between 700-NVP and 700-NVP/C, 700-NVP/C particles were finer than 700-NVP. On 800-NVP particles (Figure 3g), the observed particle sizes of 800-NVP are of 5.0-30 μm. Compared with 700-NVP, the particles of 800-NVP became enormous as the temperature increases. Additionally, the sample of 900-NVP was melted.

(a)

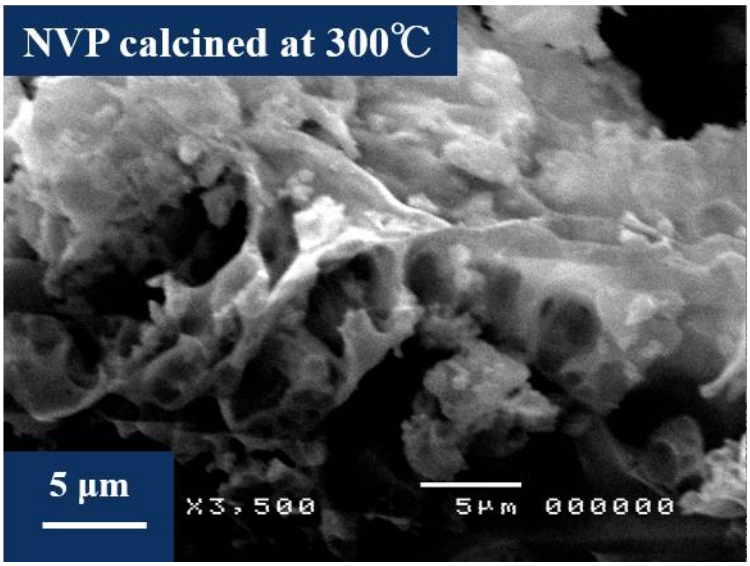
NVP calcined at 300℃
5 μm
X3,500
5μm 000000

(b)

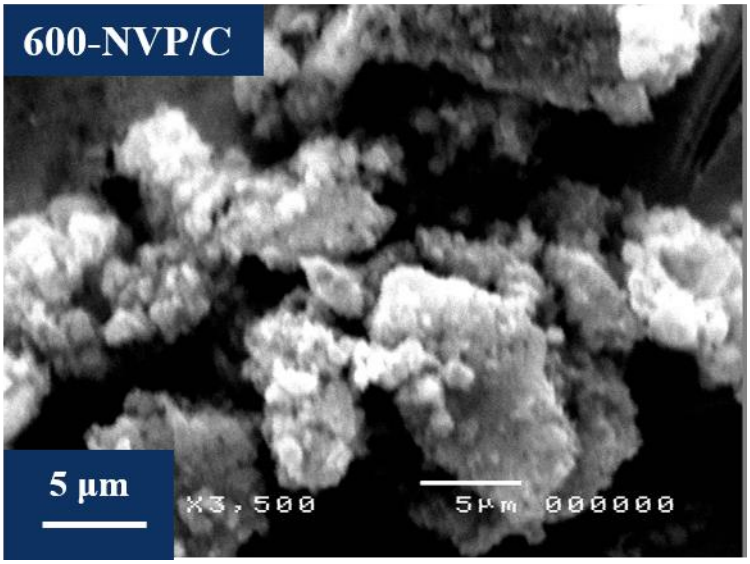
600-NVP/C
5 μm
X3,500
5μm 000000

(c)

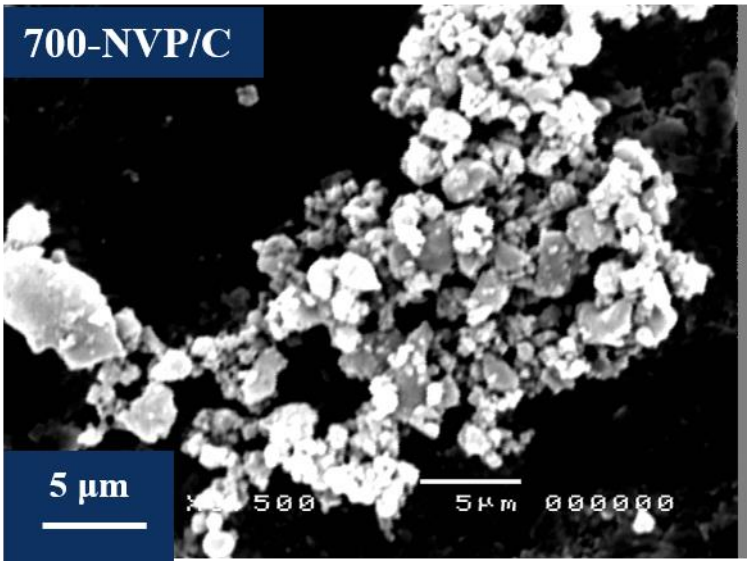
700-NVP/C
5 μm
5μm 000000

(d)

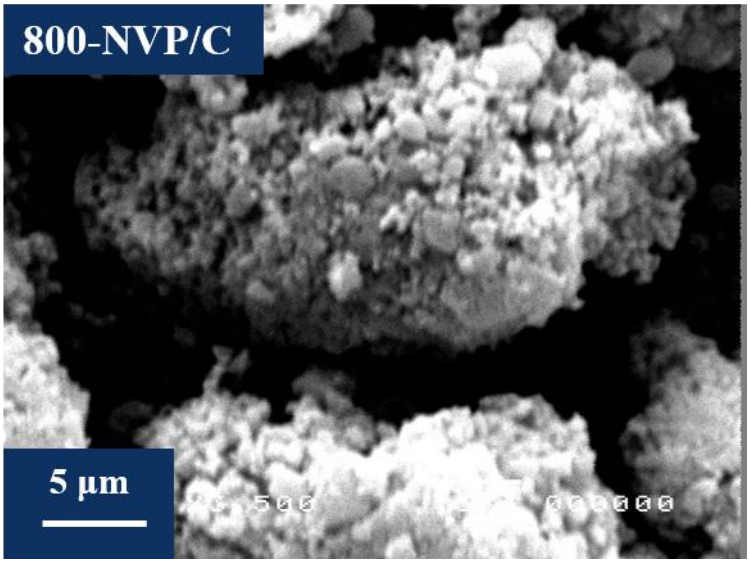
800-NVP/C
5 µm

(e)

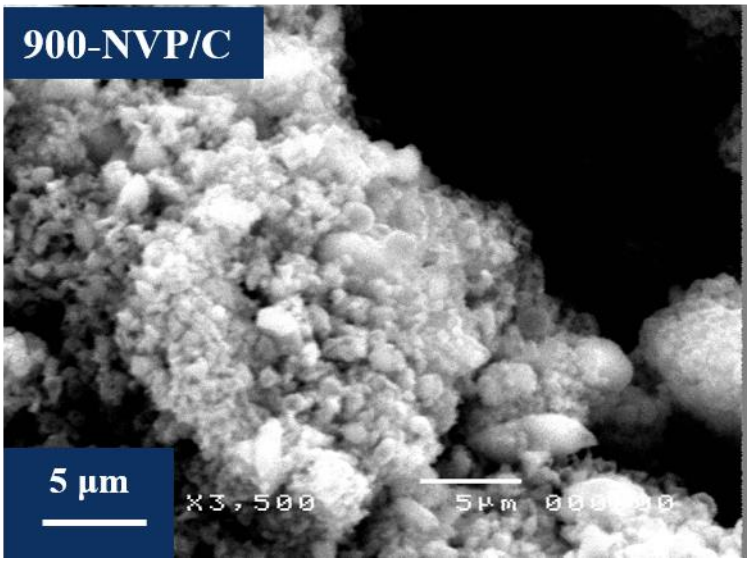
900-NVP/C
5 µm
X3,500
5µm

(f)

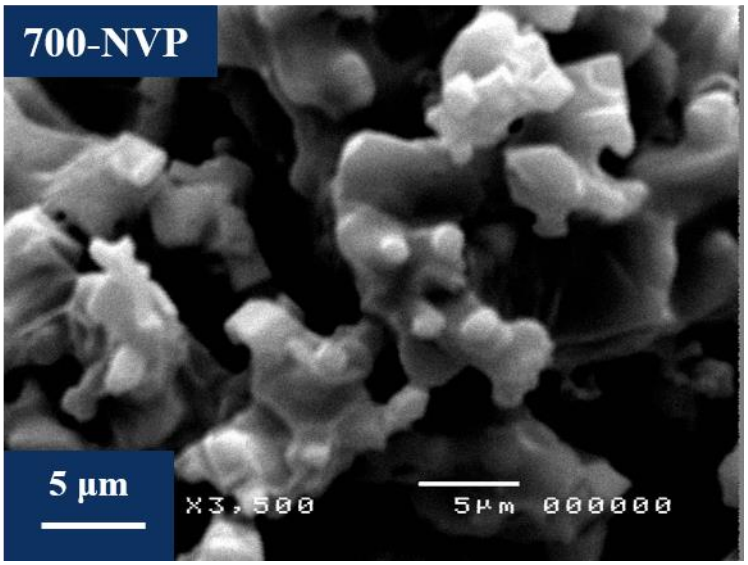
700-NVP
5 µm
X3,500
5µm 000000

(g)

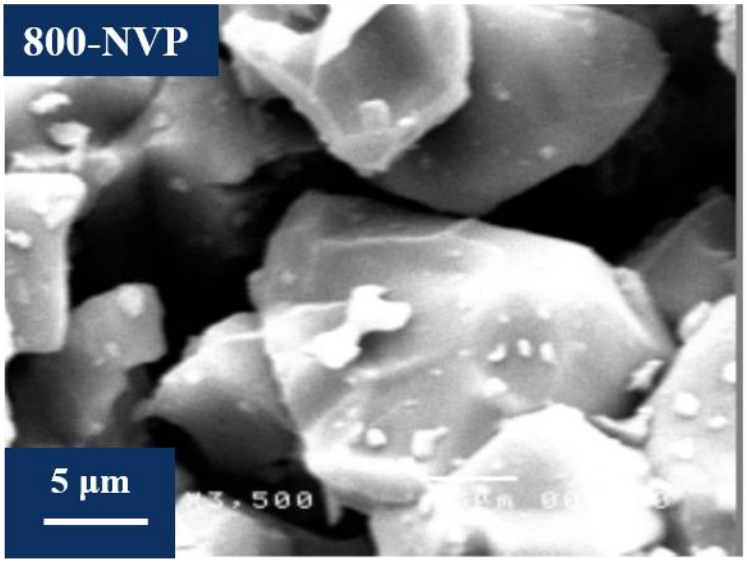

Figure 3. SEM images of (a) intermediate product of $Na_3V_2(PO_4)_3$ calcined at 300ºC, $Na_3V_2(PO_4)_3$/C synthesized with polystyrene calcined at (b) 600ºC, (c) 700ºC , (d) 800ºC and (e) 900ºC , and $Na_3V_2(PO_4)_3$ synthesized without polystyrene at (f) 700ºC and (g) 800ºC.

To clarify the particle size and the morphology of particle surface carbon layer, we performed the TEM observation of the NVP/C samples (Figure 4). The particle size of each sample is about 100 nm or larger. For all the NVP/C samples, it is confirmed that the NVP particle surfaces were covered with carbon layers. The thickness of carbon layer of 600-NVP/C, 700-NVP/C, 800-NVP/C and 900-NVP/C are found to be 3.5 nm, 3.9 nm, 3.1 nm and 2.9 nm, respectively. The particle surfaces of 800-NVP/C and 900-NVP/C were covered with partial, non-uniform carbon layers, contrast to 600-NVP/C and 700-NVP/C. In the figures, smoke-like carbons can be seen the space among NVP particles, and with increasing calcination temperatures, the carbons are likely to grow up from space to space. In contrast, for the samples calcined at relatively low temperatures such 600-NVP/C and 700-NVP/C, the smoke-like carbons seems to disappear. These phenomena imply that, due to rapid decomposition reaction of polystyrene at high temperatures, some parts of generated carbons aggregate to be smoke-like carbons otherwise to be deposited on NVP particles.

The surface areas of 600-NVP/C, 700-NVP/C, 800-NVP/C and 900-NVP/C are 14.4 $m^2 g^{-1}$, 12.3 $m^2 g^{-1}$, 11.2 $m^2 g^{-1}$ and 11.9 $m^2 g^{-1}$, respectively. It could be reasonable that the carbon materials on particle surfaces have only limited effects in surface area measurements because of quite low amounts of carbon layers on NVP particles. On increasing temperature from 600 to 700°C, the decrease in surface area is observed. The fact means that the particles slightly grow with increase in temperature. On the other hand, with increasing calcination temperature over 700°C, there is somewhat different behavior, i.e., almost constant surface area. These results are consistent with the tendency of TEM observation that indicated the particle sizes of the samples are not too much different one another even calcined at various temperatures.

(a)

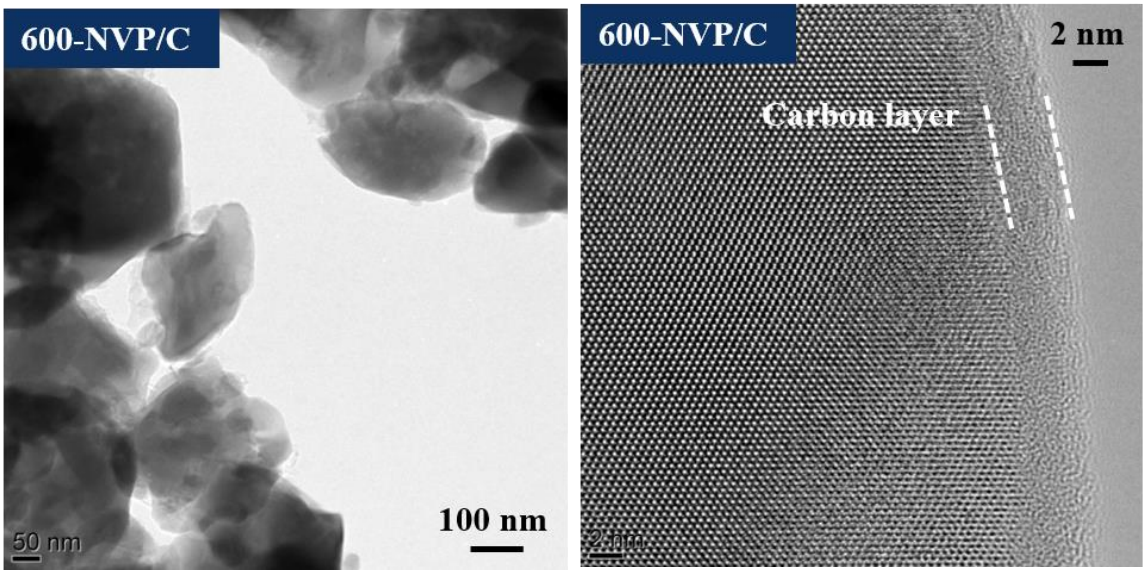
600-NVP/C
100 nm
50 nm
600-NVP/C
2 nm
Carbon layer
2 nm

(b)

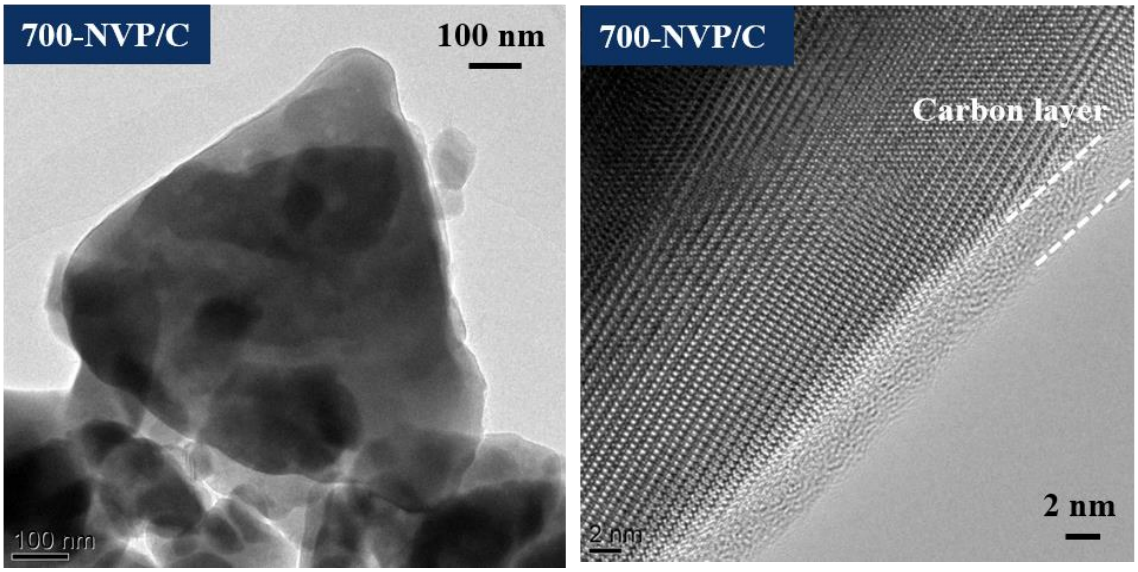
700-NVP/C
100 nm
100 nm
700-NVP/C
Carbon layer
2 nm
2 nm

(c)

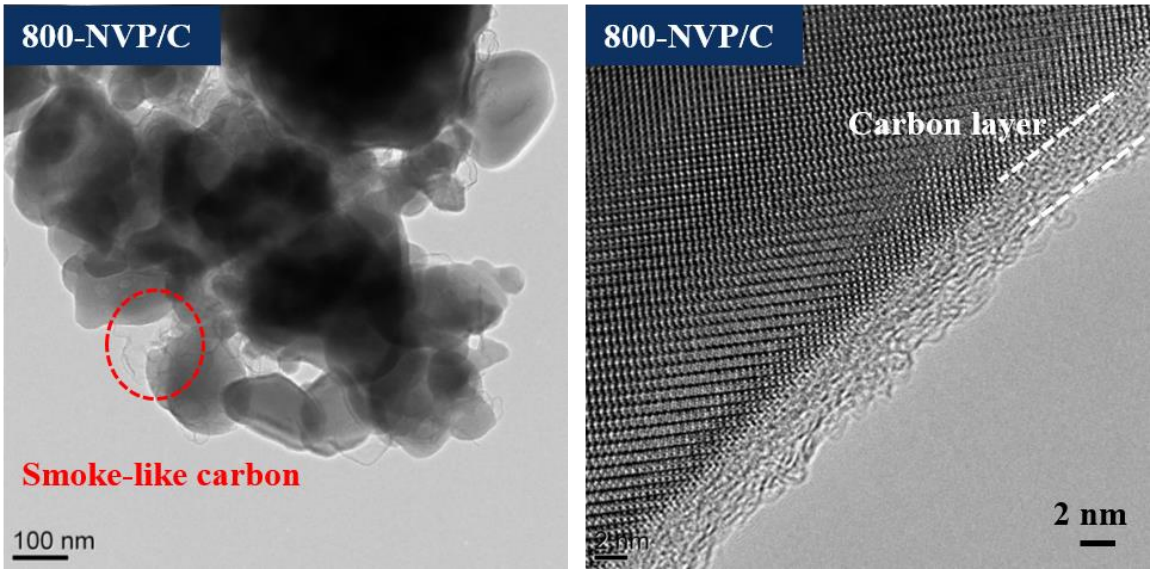

(d)

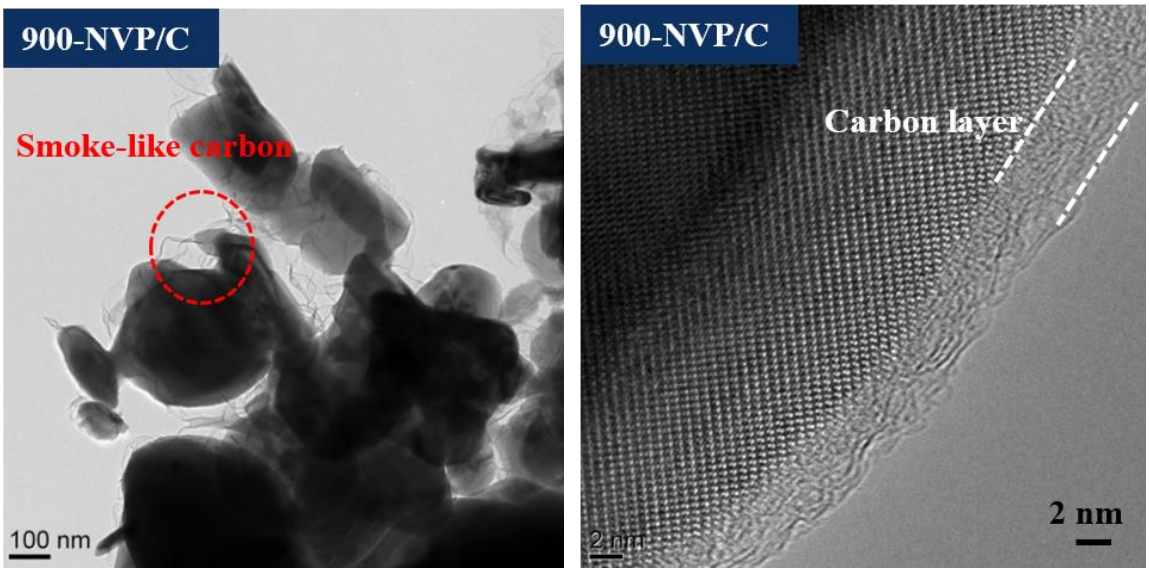

Figure 4. TEM images of $Na_3V_2(PO_4)_3$/C synthesized with polystyrene at calcine temperatures of (a) 600ºC, (b) 700ºC, (c) 800ºC and (d) 900ºC.

Raman spectroscopy measurements were carried out to detect existence of carbon and morphologies of carbon, i.e., sp^2- or sp^3-carbon, on NVP particle surfaces. Figure 5a shows Raman spectra of non-carbon-coated NVP. We can see two intense peaks at 450 and 1050 cm^{-1} and a broad peak at 570 cm^{-1}, all of which are attributed from vibration modes of $Na_3V_2(PO_4)_3$. Figure 5b shows Raman spectra of carbon-coated samples of NVP/C. We can observe a peak at 1600 cm^{-1} (G band, sp^2-like graphitic carbon) and a peak at 1350 cm^{-1} (D band, sp^3-like disordered carbon).[40] In the Raman spectra of 600-NVP/C, in addition to two peaks of G band and D band, another two peaks at 450 and 1050 cm^{-1} that belong to NVP lattice can be seen with relatively high intensity. Additionally, another peak is identified at around 950 cm^{-1}, due to $(PO_4)^{3-}$. In the Raman spectra of 700-NVP/C, two peaks attributed to G band and D band are clearly observed, but peaks attributed to NVP lattice are barely detectable. However, as is the case with 600-NVP/C, the peak appeared at around 950 cm^{-1} is conformably detectable. In the Raman spectra of 800-NVP/C and 900-NVP/C, two peaks attributed to G band and D band are clearly shown, and the other peaks are also seen at 450 and 1030 cm^{-1} attributed to NVP lattice. Especially, two peaks at 450 and 1030 cm^{-1} of 900-NVP/C are relatively intense. This means the existence of bare surfaces that is not covered with carbon. The proportion of graphitic carbon in the total amount of generated carbon materials was evaluated from Raman spectra by the least square calculations of peak profile fitting. The proportions of 600-NVP/C, 700-NVP/C, 800-NVP/C and 900-NVP/C were 23 %, 26 %, 26 % and 29 %, respectively. This result may be indicative that the higher temperature the calcination is taken place at, the more graphitic carbon can be obtained. Here, from results of Raman spectroscopy, it is suggested that too high calcination temperature gives rise to deficient carbon layers.

The TEM observation for 600-NVP/C clarifies that NVP particles were covered with carbon layers and smoke-like carbon materials were present in inter-particle spaces with a very small amount. However, the Raman spectra suggests the existence of relatively large amounts of bare NVP particles. Therefore, it could be concluded that the particles of 600-NVP/C cannot be covered with carbon layers uniformly. The TEM observation for 700-NVP/C samples reveals existence of carbon layers on NVP particle surfaces without smoke-like carbon. The information obtained from the Raman spectra indicates little signal from NVP itself. Therefore, the surfaces of 700-NVP/C particles were covered with smooth carbon layers uniformly. On

the other hand, the TEM observations for 800-NVP/C and 900-NVP/C indicate that these particles were also covered with carbon layers, but smoke-like carbon materials were present between NVP particles. In the Raman spectra, the signals due to bare NVP particles are certainly observed for both samples, where the signal is more intensive for 900-NVP/C than for 800-NVP/C. In conclusion, it should be noted that carbon layers of 800-NVP/C and 900-NVP/C can cover partially the particle surface but not extend to cover the whole surface completely.

(a)

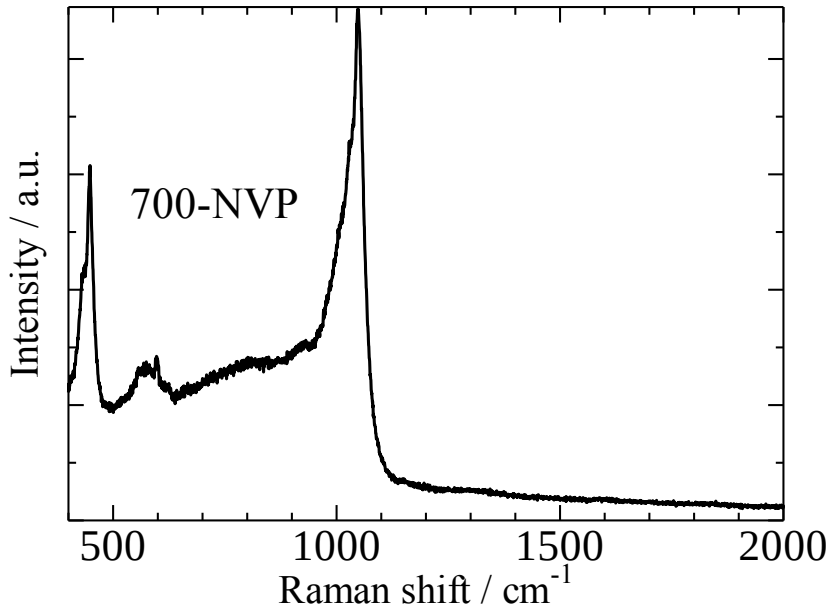

(b)

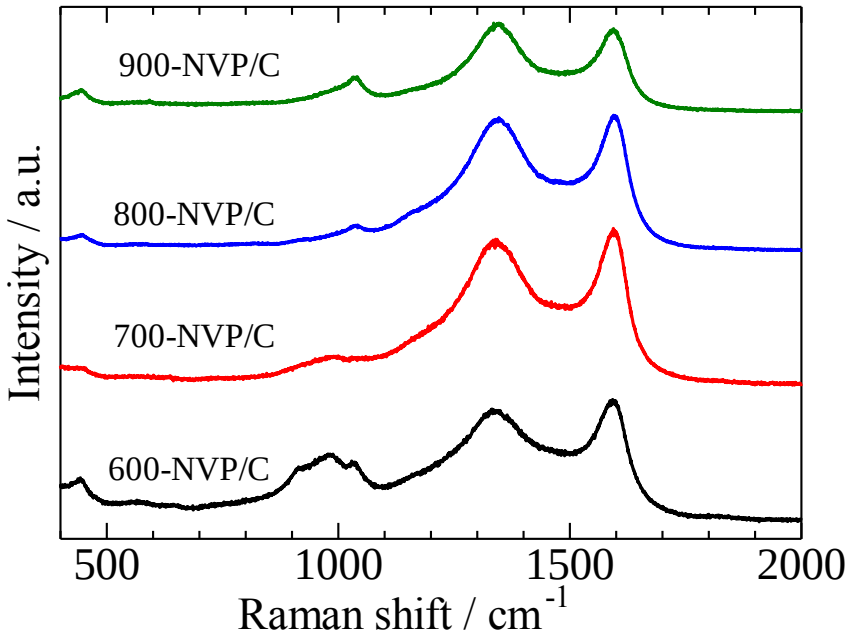

Figure5. Raman spectra of (a) intermediate product of $Na_3V_2(PO_4)_3$ calcined at 700ºC and (b) $Na_3V_2(PO_4)_3$/C synthesized with polystyrene at calcine temperatures from 600 to 900ºC.

Table 2. Proportion of graphitic carbon to generated total carbon materials [G band / (G band + D band)].

Sample	600-NVP/C	700-NVP/C	800-NVP/C	900-NVP/C
Ratio of graphite (%) [G band / (G band + D band)]	23	26	26	29

The charge and discharge measurements of carbon-coated NVP/C samples were conducted at the current densities from 0.5 to 5C. Figure 6a shows charge-discharge profiles operated at 0.5C for the samples synthesized at various calcination temperatures. In these samples, at 2.5 V, The discharge capacities at the voltage down to 2.5 V for 600-NVP/C, 700-NVP/C, 800-NVP/C and 900-NVP/C 700-NVP/C were 91, 121, 121 and 116 mAh g^{-1}, respectively. The discharge capacities are acceptable levels compared with the theoretical capacity of 118 mAh g^{-1}, corresponding to two Na ions extraction in the range of 2.5 - 3.7 V.[35] The samples of 700-NVP/C and 800-NVP/C exhibited the highest discharge capacity. The sample of 600-NVP/C recorded the lowest discharge capacity. Figure 6b shows charge-discharge profiles obtained for 600-NVP/C at every fifth charge-discharge cycles conducted at the C rates from 0.5C to 5C. Discharge capacity of 600-NVP/C at 1 and 2C were 71 and 46 mAh g^{-1}, respectively. In the sample, discharge capacities fairly low at each C rate compared with those of the other samples, and charge-discharge measurement couldn't be conducted at 5C. As shown in Figure 6c, the sample of 700-NVP/C indicates the best charge-discharge performance in these samples.[19] The discharge capacity of 800-NVP/C (Figure 6d) shows enough high at 0.5 and 1C, though the discharge capacity above these rate decreases with an increase in current density. The discharge capacity of 900-NVP/C (Figure 6e) shows relatively high, but low at high current densities. The charge-discharge measurement couldn't be conduct at 5C.

(a)

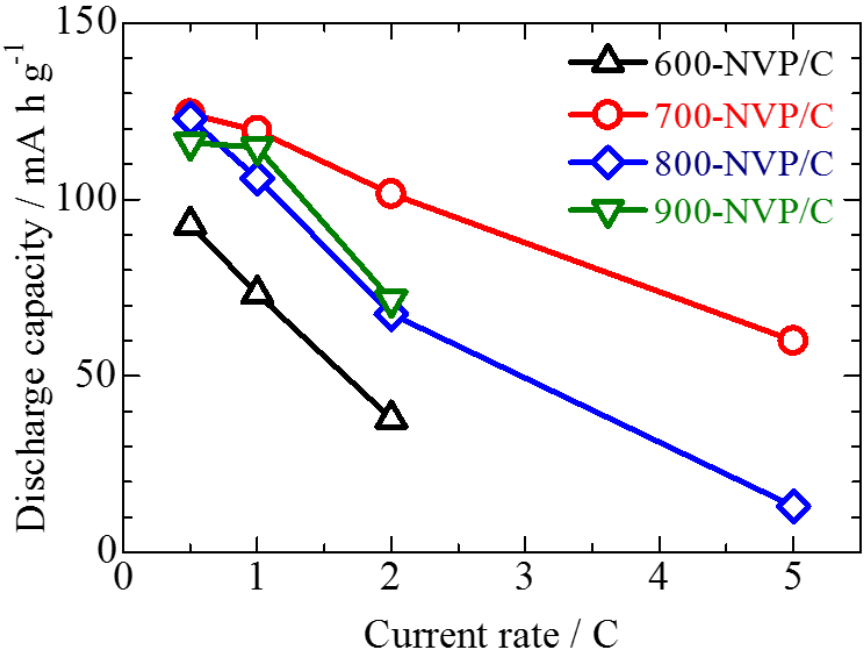
Discharge capacity / mA h g-1
Current rate / C
600-NVP/C
700-NVP/C
800-NVP/C
900-NVP/C
0
50
100
150
0
1
2
3
4
5

(b)

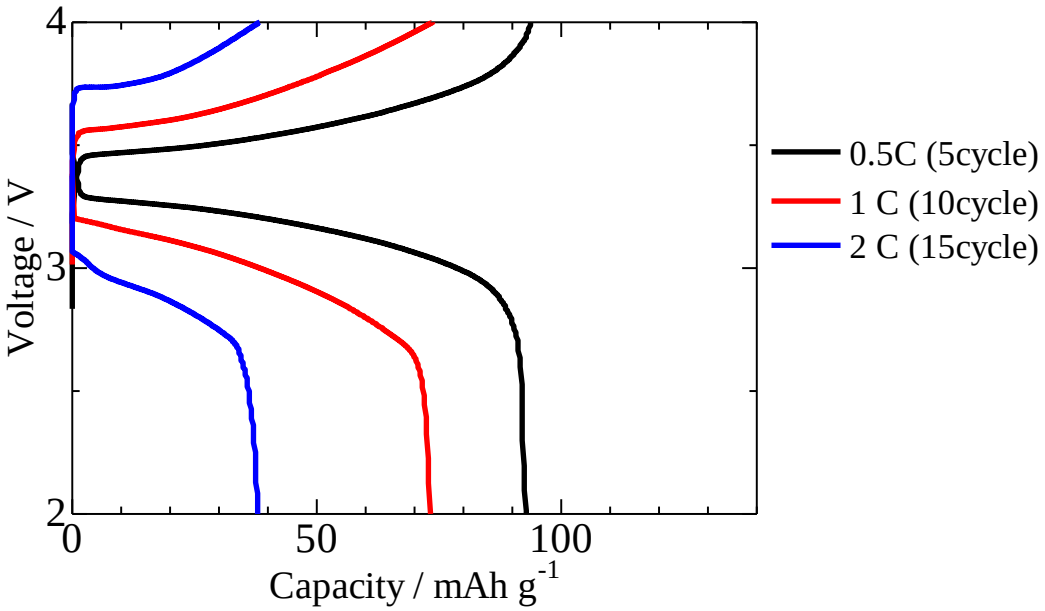
Voltage / V
Capacity / mAh g-1
0.5C (5cycle)
1 C (10cycle)
2 C (15cycle)
2
3
4
0
50
100

(c)

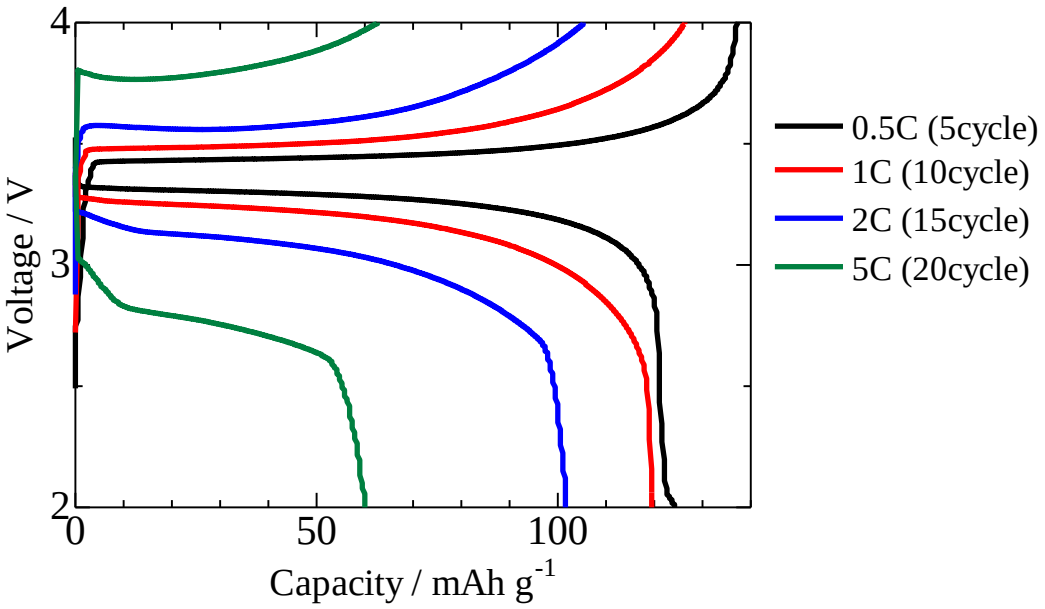
4
3
2
Voltage / V
0
50
100
Capacity / mAh g-1
0.5C (5cycle)
1C (10cycle)
2C (15cycle)
5C (20cycle)

(d)

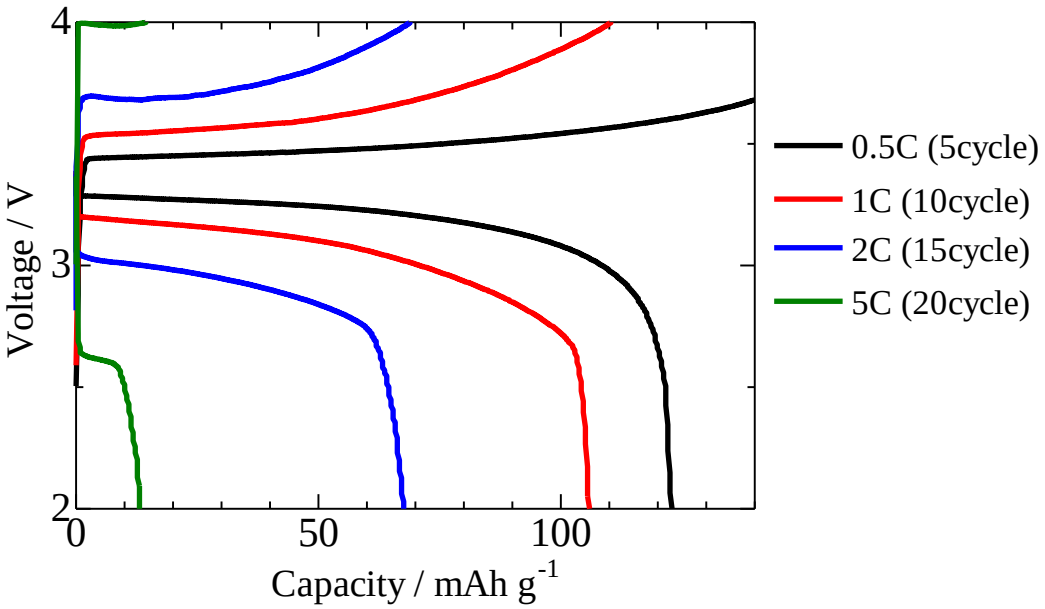
4
3
2
Voltage / V
0
50
100
Capacity / mAh g-1
0.5C (5cycle)
1C (10cycle)
2C (15cycle)
5C (20cycle)

(e)

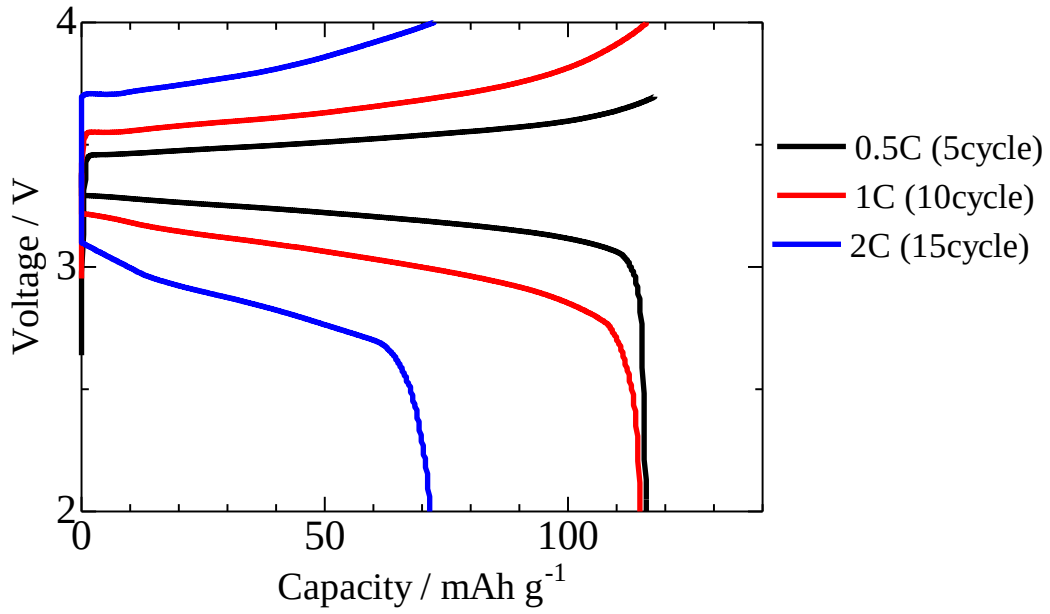

Figure 6. (a) Rate performance of $Na_3V_2(PO_4)_3$/C synthesized with polystyrene at calcination temperatures from 600 to 900ºC and charge-discharge curves of $Na_3V_2(PO_4)_3$/C synthesized at calcination temperatures of (b) 600ºC , (c) 700ºC , (d) 800ºC and (e) 900ºC.

As shown in Figure 6, the beat electrochemical performance was obtained for the sample of 700-NVP/C among all the samples investigated. This is because the sample 700-NVP/C has low proportion of $NaVP_2O_7$ impurity phase as well as uniform carbon coating layers on the particle surfaces. It could be concluded that these factors are the most important to improve electrochemical property of NVP. In general, not only phase purity of active cathode materials but also electrical conductivity of the active materials are key issues for acquisition of excellent battery properties.

Raman spectra of 800-NVP/C and 900-NVP/C indicate clear peaks due to NVP lattice, where much intense NVP peaks are confirmed for the sample of 900-NVP/C. In terms of carbon coating, the results of Raman spectra imply that the particle surfaces of 800-NVP/C and 900-NVP/C were covered with partially non-uniform carbon layers. Probably, carbon coating of 900-NVP/C was not enough. TEM observation also implies that, the particle surfaces of 800-NVP/C and 900-NVP/C were covered with partially non-uniform carbon layers. In charge-discharge measurements, the 900-NVP/C sample shows a relatively favorable discharge capacity at 0.5C but an abrupt deterioration in discharge capacity is observed at high current densities. The discharge capacity of 800-NVP/C is superior at low current densities and gradual deterioration in battery performance is observed at high current densities, compared to the results of 900-NVP/C. In other words, 800-NVP/C can maintain good discharge property in some degree, compared to 900-NVP/C, because deposited carbon layers on 800-NVP/C particles can keep relatively better conductive conditions. This symptom is considered that Na ion diffusion at phase boundaries between particle surfaces deteriorates because of lower electronic conductivity attributed to insufficient carbon coating.

The sample of 600-NVP/C has clear G band and D band peaks in the Raman spectra, and also has peaks due to NVP lattice. The TEM observation for 600-NVP/C implies that the particles are certainly covered with carbon layers. In fact, a small amount of the smoke-like carbon materials are present in the spaces among particles. Though the discharge capacity of the sample is measurable at low current densities but is no more conducted at 5C. According to the Raman spectra, insufficient electronic conductivity associated with insufficient coating of carbon layers was evaluated from the intensive peaks due to NVP lattice. Therefore, the poor performance observed for the sample of 600-NVP/C is concluded to be due to non-uniform

carbon deposition on particle surfaces.

The sample of 600-NVP/C shows the worse charge-discharge performance among all the samples. Any notable impurities, such a $NaVP_2O_7$ phase, are detected in the XRD measurements. The Rietveld refinements reveal that the samples of 800-NVP/C and 900-NVP/C have larger proportion of $NaVP_2O_7$ than the samples of 600-NVP/C or 700-NVP/C. However, the sample of 800-NVP/C shows superior charge-discharge performance compared to the sample of 600-NVP/C. Moreover, the samples of 900-NVP/C shows superior charge-discharge performance compared to the sample of 600-NVP/C. Hence, deterioration of discharge performance property for 600-NVP/C is not due to the existence of $NaVP_2O_7$.

From the Rietveld refinement, it should be concluded that the sample of 700-NVP/C has quite low impurity proportion of $NaVP_2O_7$. In addition, the results of Raman spectroscopy reveal that particle surfaces were covered with uniform carbon layers. Moreover, from the perspective of the charge-discharge measurements, the sample of 700-NVP/C exhibits good charge-discharge performance among all the samples. This fact seems to be due to uniform carbon coating and a small amount of impurity phase of $NaVP_2O_7$. The TEM observation for the sample of 700-NVP/C indicates that both the uniform carbon layers on the particles and less existence of the smoke-like carbon materials are accomplished. In the synthetic reaction, the decomposed precursor for NVP was ball-milled before high temperature calcinations to acquire fine particles. Additionally, polystyrene was added into the precursor and mixed, and after then crushed and calcined. When the precursor is heated at high temperatures for synthesis, only a portion of polystyrene will be converted into carbon materials. Nevertheless, as in the case of 800-NVP/C and 900-NVP/C, the generated carbon materials were not only deposited on particle surfaces but also aggregated around particles as smoke-like carbon materials. So, all the mass of polystyrene on the precursor particles does not necessarily change into carbon layers on particle surfaces. These considerations imply that the driving force behind the deposition of carbon as coating layers has some kind of relationship with inhibition in crystallization of $NaVP_2O_7$.

3.2. Improvement of High Rate Performances for Ti-Doped $Li_3V_2(PO_4)_3$ Cathode Materials

In the DSC curves of the non-doped sample of $Li_2V_2(PO_4)_3$ (Figure 7), two characteristic peaks were clearly observed at around 110 and 180°C (exothermic) and at 120 and 185°C (endothermic), indicating the temperature dependent phase transitions from monoclinic to orthorhombic. However, no reversible transitions were seen for the Ti-substituted samples ($x \geq 0.025$). Referring to our previous work,[5] two reversible phase transitions observed are considered to be due to the $\alpha \rightarrow \beta$ and $\beta \rightarrow \gamma$ phases transitions, respectively.

On the other hand, from the XRD patterns of $Li_{3-2x}(V_{1-x}Ti_x)_2(PO_4)_3/C$ (x=0, 0.025, 0.050, 0.10, 0.20) (Figure 8), it was confirmed that all samples consist of a single phase. Making the comparison of the XRD pattern from ICSD date, the minor peak characteristic of orthorhombic $Li_2(Ti)_2(PO_4)_3$ at 24° emerged with increasing Ti more than x = 0.10, while the minor peak characteristic of monoclinic $Li_3V_2(PO_4)_3/C$ at 37° faded with increasing Ti more than x = 0.10. These results suggest that the $Li_{3-2x}(V_{1-x}Ti_x)_2(PO_4)_3/C$ samples with the Ti substitution ratios above x = 0.10 stabilize in the orthorhombic γ-phase at room temperature.

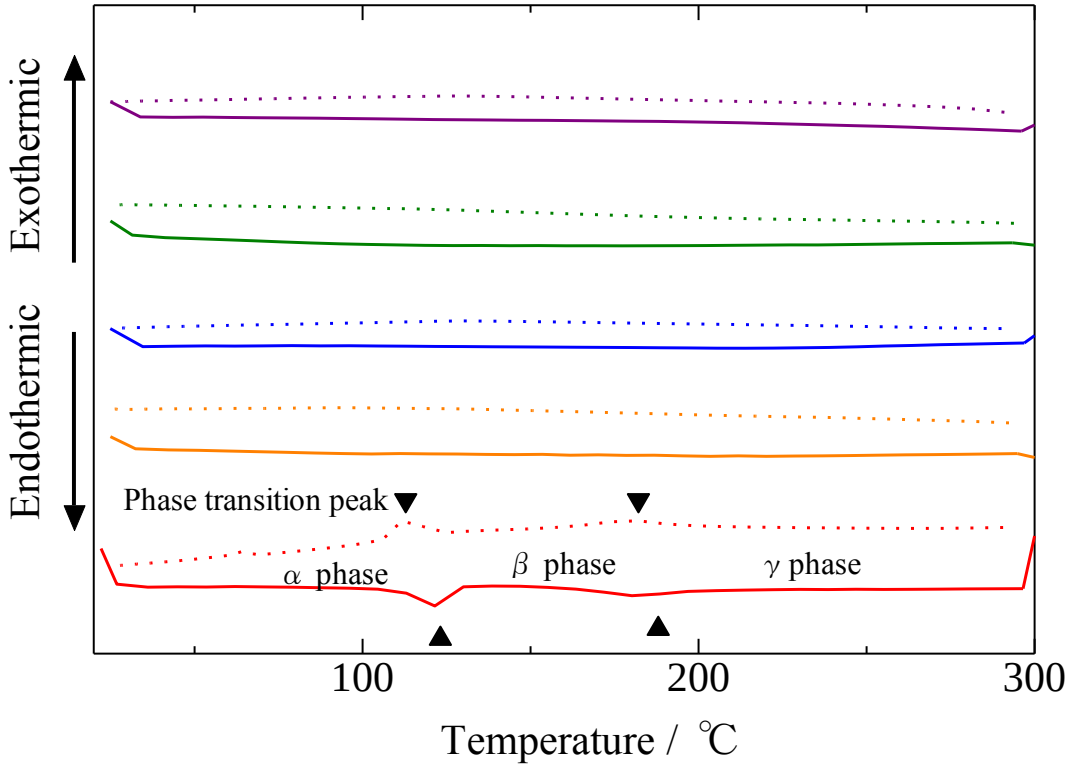

Figure 7. DSC curves of $Li_{3-2x}(V_{1-x}Ti_x)_2(PO_4)_3$/C: x=0 (red), 0.025 (orange), 0.050 (blue), 0.10 (green), and 0.2 (purple). The solid and broken lines represent the stages of the temperature rising and cooling, respectively.

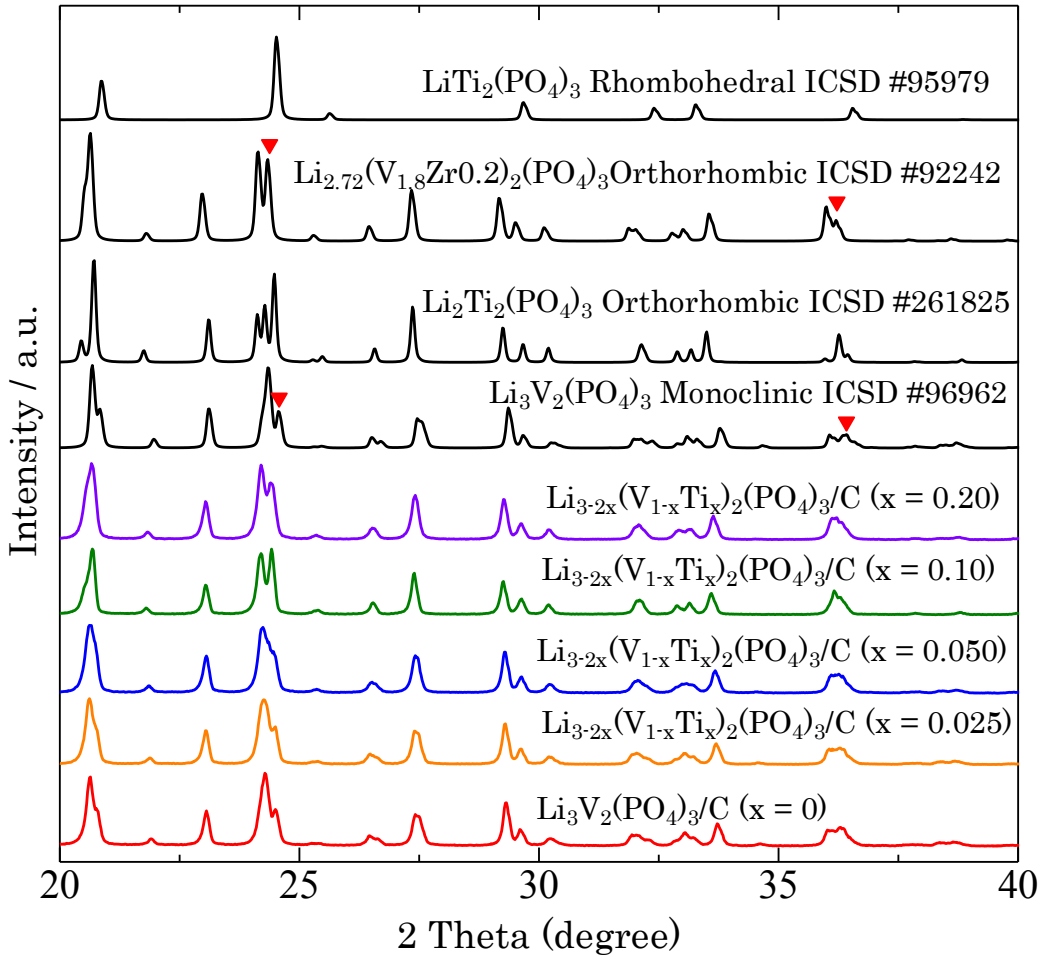

Figure 8. XRD patterns of $Li_{3-2x}(V_{1-x}Ti_x)_2(PO_4)_3/C$ (x = 0, 0.025, 0.050, 0.10, 0.20) prepared.

The variations in the temperature dependence of the conductivity for no-carbon-coated $Li_{3-2x}(V_{1-x}Ti_x)_2(PO_4)_3$ are illustrated in Figure 9. When taking notice of the region where the high temperature phase (i.e., γ-phase) is stable, the $Li_{3-2x}(V_{1-x}Ti_x)_2(PO_4)_3$ (x = 0.10, 0.20) samples are apparent to have a linear dependence of log σ versus $1/T$ and also to show almost the same slope as that of the γ-phase of $Li_3V_2(PO_4)_3$ (x = 0), also indicating the stabilization of the γ-phase at room temperature.[5] However, in the regions where the low and middle temperature phases are stable, the details of conductivity behavior remained unknown at present because of lack of enough data points. On the other hand, $Li_{3-2x}(V_{1-x}Ti_x)_2(PO_4)_3$ (x = 0.025, 0.050) do not exhibit the same tendency as $Li_3V_2(PO_4)_3$ (x = 0) at the high temperature region. Such findings are consistent with those of Figure 8. In comparison with the profile of the DSC curves, both XRD patterns and results of the conductivity imply that the stabilization of the γ-phase occurred at the substitution ratio over x = 0.10. This consequence present that fractional Ti doping has effect on prohibition of temperature dependence phase transition, but it seemed to say that the necessary quantity of Ti doping for stabilization is higher than the results of the DSC analysis.

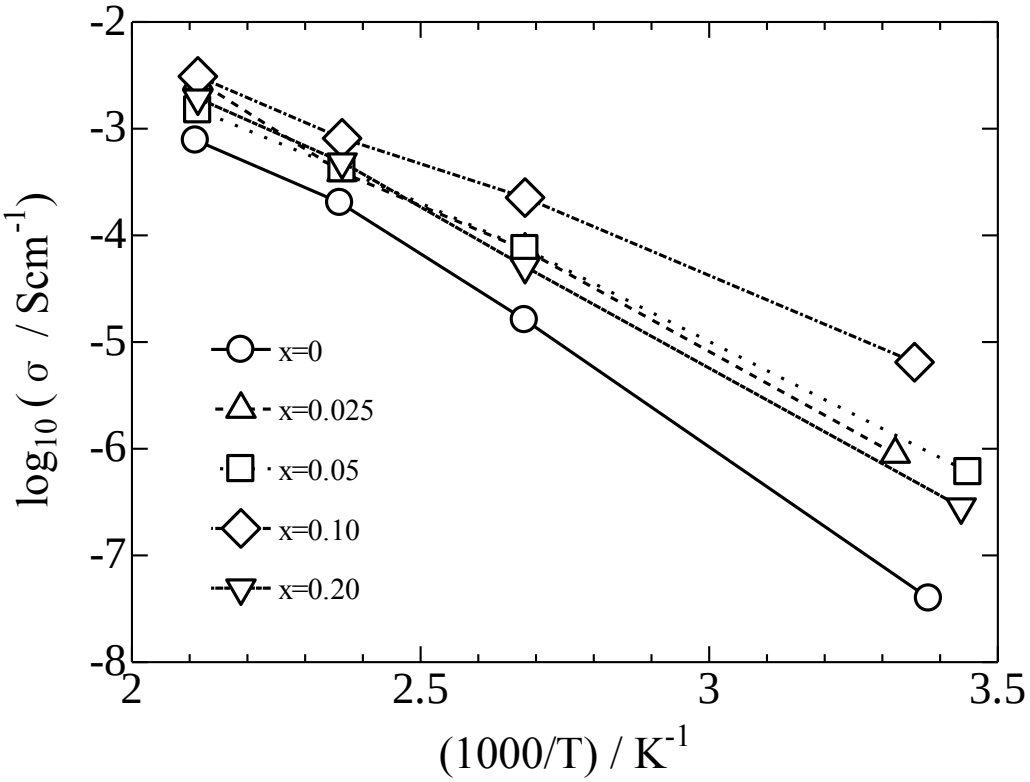

Figure 9. Temperature dependence of electrical conductivity of $Li_{3-2x}(V_{1-x}Ti_x)_2(PO_4)_3$.

To clarify the particle sizes and the conditions of surface carbon layers, we performed the TEM observation for the sample of $Li_{3-2x}(V_{1-x}Ti_x)_2(PO_4)_3/C$. Figure 10 shows the TEM images, showing that the particle sizes of the samples are almost equal, larger than 100 nm and covered with the carbon layers. On the particle surface except for $x = 0.025$, the thick carbon layers are deposited with the sizes from about 4 to 6 nm. On the other hand, the thickness of the carbon layer for the sample with $x = 0.025$ is in the range from about 8 to 10 nm.[42–45] One possible reason for this probably comes from its composition which lies in the Ti-substitution ratio that determines the stabilization of the γ-phase at room temperature, i.e., the sample with $x = 0.025$ consisting of the α-phase and γ-phase, but the details are unknown at present. In addition, the laminate structure of graphite is hardly seen on the particle surface of the sample with $x = 0.025$. In contrast, the laminate structure of graphite on the particle surface and phase boundary is clearly observed for the sample with $x = 0.20$. The results suggest that the amount of Ti dopant has an impact on the deposition of carbon materials on particle surface. In the figures, the smoke-like carbons between particles and/or on particle surfaces are confirmed for all the Ti substituted samples.

(a)

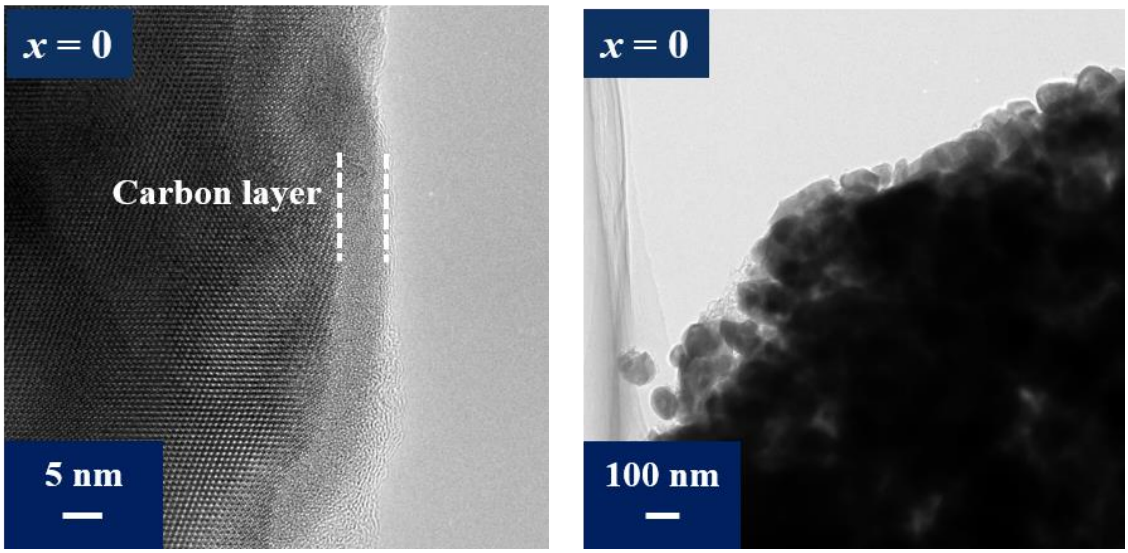
x = 0
Carbon layer
5 nm
x = 0
100 nm

(b)

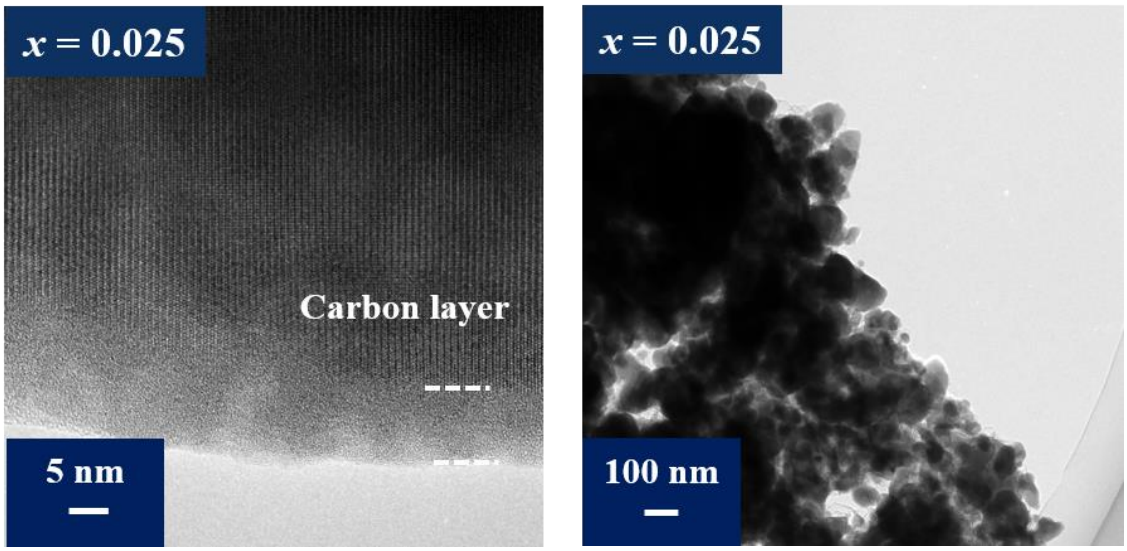
x = 0.025
Carbon layer
5 nm
x = 0.025
100 nm

(c)

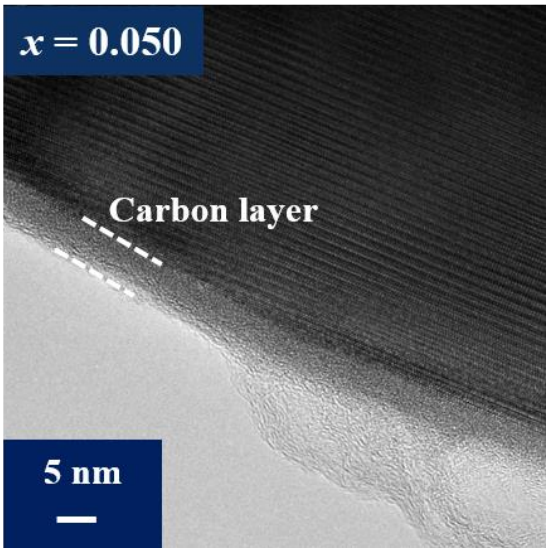
x = 0.050
Carbon layer
5 nm

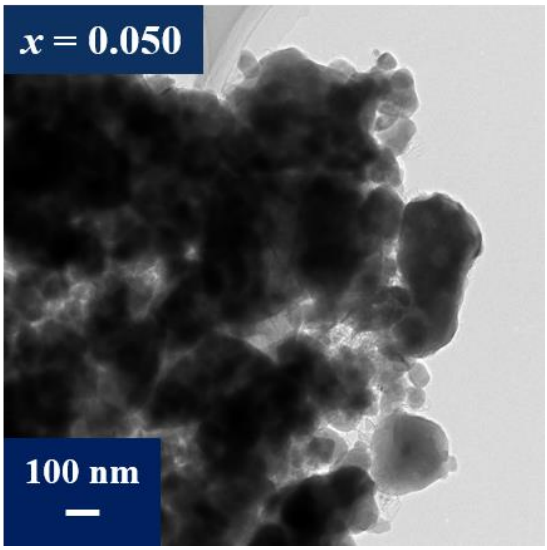
x = 0.050
100 nm

(d)

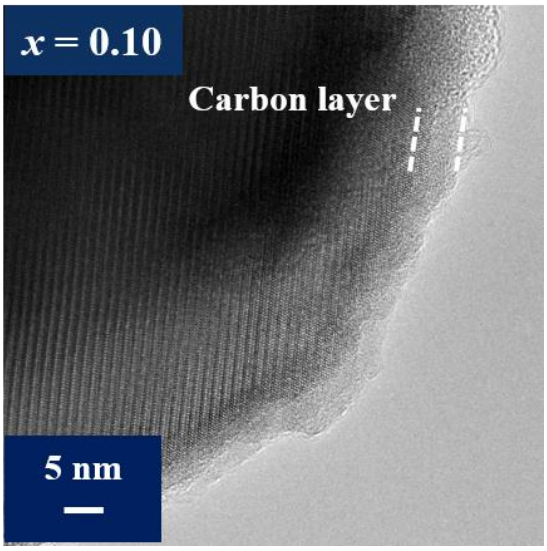
x = 0.10
Carbon layer
5 nm

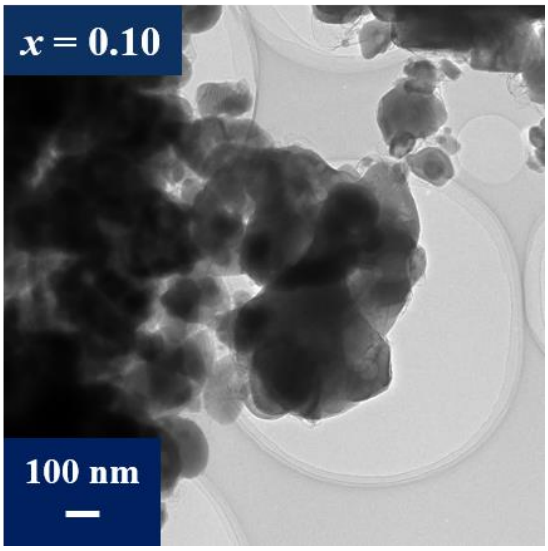
x = 0.10
100 nm

(e)

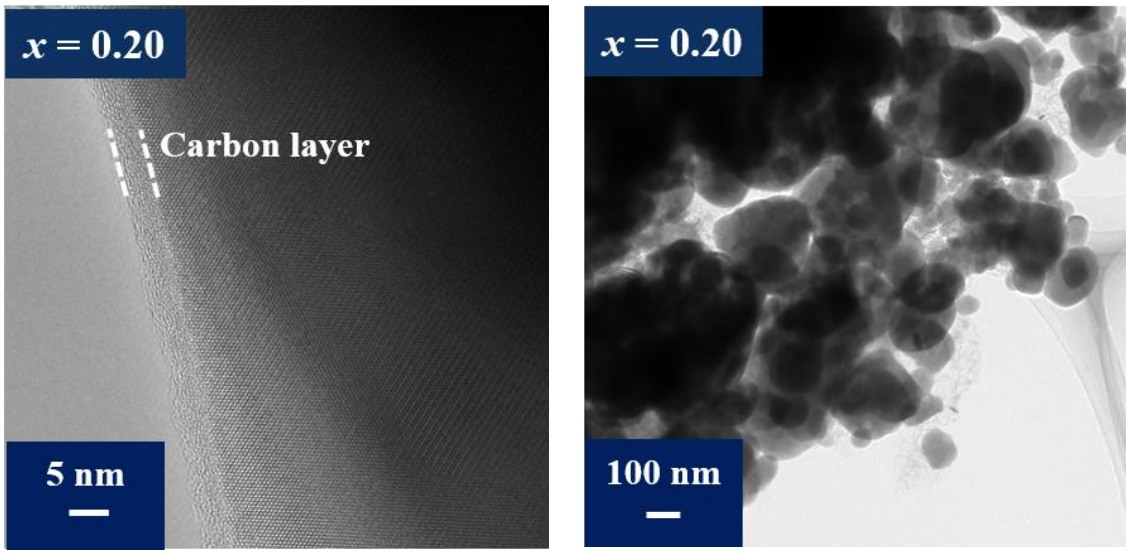

Figure 10. HRTEM images of the $Li_{3-2x}(V_{1-x}Ti_x)_2(PO_4)_3$/C samples carbon-coated with (a) x = 0, (b) x = 0.025 , (c) x = 0.050, (d) x = 0.10 and (e) x = 0.20.

Figure 11 shows the charge-discharge curves of $Li_{3-2x}(V_{1-x}Ti_x)_2(PO_4)_3$/C at 0.2C in the voltage range between 2.0 and 4.8 V. For $Li_{3-2x}(V_{1-x}Ti_x)_2(PO_4)_3$/C ($x$ = 0, 0.025, 0.050), the discharge capacities at 3.0 at V are found to be about 160 mAh g^{-1}, whereas about 154 mAh g^{-1} for the samples with x = 0.10 and 0.20. The charge curves apparently exhibit four plateaus (3.60, 3.68, 4.08, and 4.63 V) that imply the phase transitions based on 3Li delivery, in contrast, the discharge ones are of wavelike curves. It is clear from such discharge curves that 3Li migration scarcely reflects on the appearance of plateau; the discharge curves for of $Li_3Ti_2(PO_4)_3$ phase show a solid solution behavior.[46,47] The sample with x = 0.2 shows an another plateaus at 2.5 V both in charge and discharge processes, indicating a redox couple of Ti^{3+}/Ti^{4+} and higher discharge capacity about 30 mAh g^{-1}.[42] In terms of charge-discharge performance, there are not clear differences among the $Li_{3-2x}(V_{1-x}Ti_x)_2(PO_4)_3$/C samples with various Ti substitution ratios. A noteworthy phenomenon is the emergence of a redox couple of Ti^{3+}/Ti^{4} observed only for the sample with x = 0.20. In Figure 11, around the charge-discharge capacity region between 70 ~ 140 mAh g^{-1}, the discharge voltage of the sample with x = 0.20 is slightly higher than those of the other samples. This result implies that Li ion diffusivity is promoted by the room temperature stabilization of the γ-phase provided by Ti doping. Moreover, it should be noted that 3Li extraction/insertion become possible for the carbon coated sampled of $Li_{3-2x}(V_{1-x}Ti_x)_2(PO_4)_3$/C. Compared with our previous work, it is apparent that the electronic conductivity of $Li_{3-2x}(V_{1-x}Ti_x)_2(PO_4)_3$/C is provided from the carbon coating.

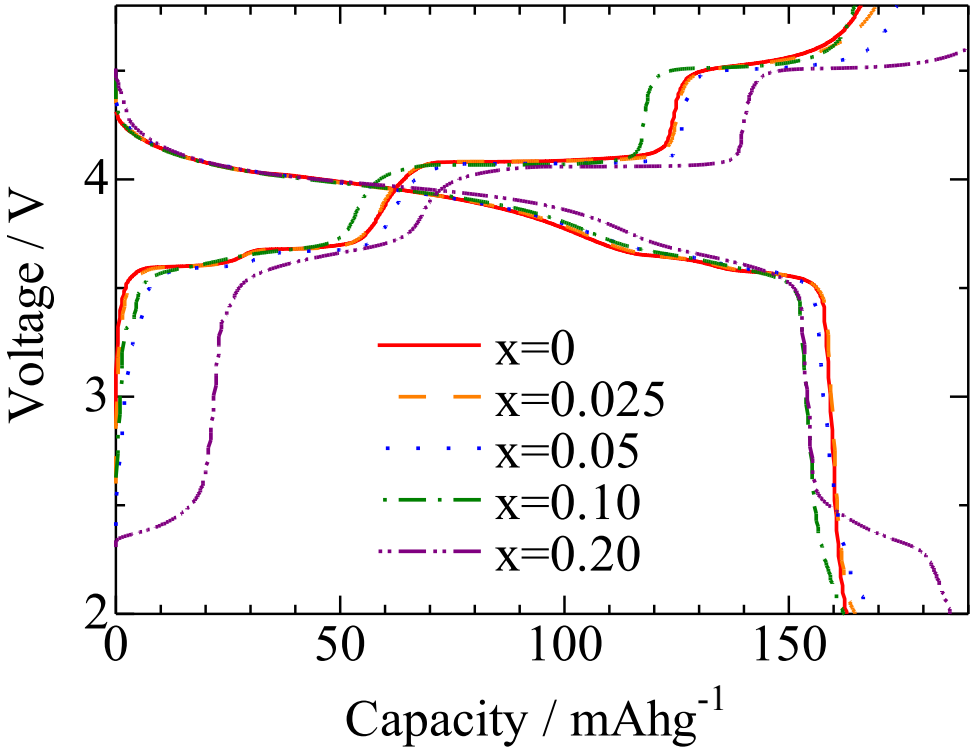

Figure 11. Charge-discharge curves of $Li_{3-2x}(V_{1-x}Ti_x)_2(PO_4)_3$/C at different C rates.

The rate performances of $Li_{3-2x}(V_{1-x}Ti_x)_2(PO_4)_3$/C were examined in the range from 0.2 to 60C. As can be seen from Figure 12, the discharge capacity are apparent to be markedly decreased in the range from 0.2 to 3C, while the capacity are dropped gradually below the theoretical capacity of 2Li delivery (132 mAh g^{-1}) over 5C. In this range, $Li_{3-2x}(V_{1-x}Ti_x)_2(PO_4)_3$/C ($x$ = 0.20) shows a comparatively higher discharge capacity than the other samples because a redox reaction of Ti^{3+}/Ti^{4+} is confirmed between 2.0 and 2.5 V.[48] When the amount of dopant Ti exceeds a constant amount about x = 0.2, two orthorhombic phases of $Li_3V_2(PO_4)_3$ and $Li_3Ti_2(PO_4)_3$ coexist in the cathode product. At 60C, the discharge capacity of $Li_3V_2(PO_4)_3$/C (x = 0) is considerably lower than that of $Li_{3-2x}(V_{1-x}Ti_x)_2(PO_4)_3$/C, indicating importance of high ionic conductivity of the γ-phase for high capacity achievement. Here, for $Li_{3-2x}(V_{1-x}Ti_x)_2(PO_4)_3$/C ($x$ = 0.025), the capacity could not be measured at 60C. In addition, from the charge-discharge performances at 0.2C measured again after 50 cycles at 60C, the decrease in the capacity are hardly observed, indicating that a robust crystal lattice of $Li_{3-2x}(V_{1-x}Ti_x)_2(PO_4)_3$/C is evident.

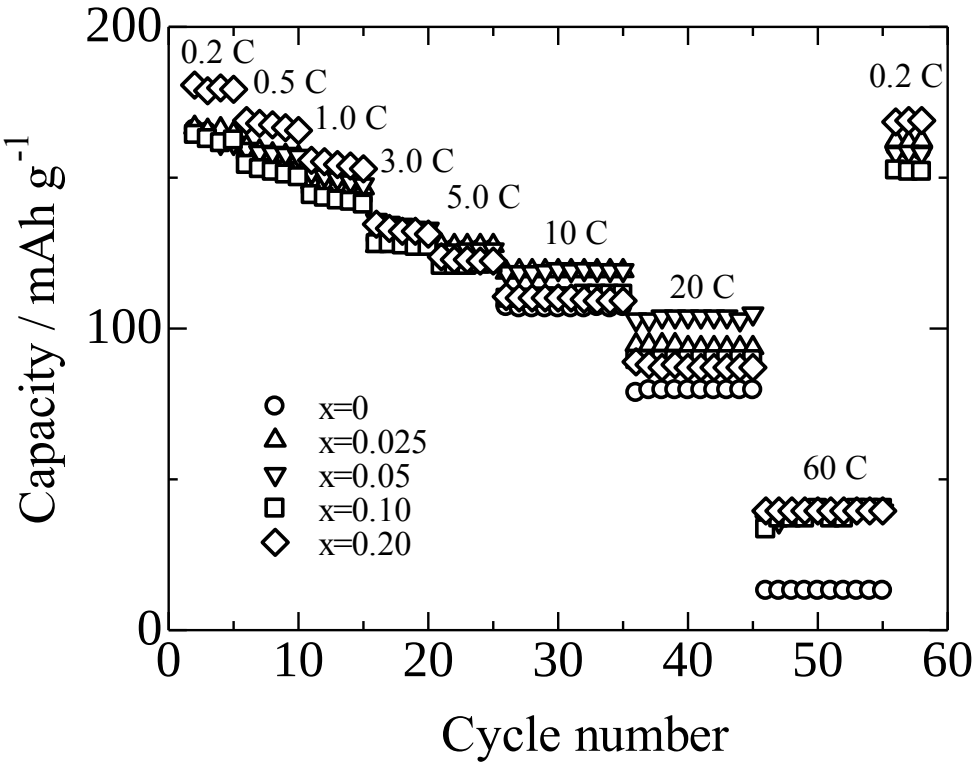

Figure 12. Rate performances of $Li_{3-2x}(V_{1-x}Ti_x)_2(PO_4)_3$/C between 0.2 and 60C.

Clearly distinguishable differences in charge-discharge performances given by the effects of Ti doping are quietly remarkable at high current densities. The discharge capacities of the sample with over $x = 0.050$ are slightly improved only at 60C. This is due to the improvement in Li ion conductivity of the stabilized γ-phase at room temperature. The effect of Ti-doping on improvement of electrochemical performance is limited. The redox reaction observed at 2.5V is an ample evidence that the impurity phase of $Li_3Ti_2(PO_4)_3$ crystallizes in $Li_{3-2x}(V_{1-x}Ti_x)_2(PO_4)_3$/C phase. The existence of $Li_3Ti_2(PO_4)_3$ is also confirmed in the XRD patterns. In addition, the TEM observation clarified clear phase boundaries and the existence of the graphitic carbon on the particle surfaces of the sample with over $x = 0.10$. This result implies that the crystallization of $Li_3Ti_2(PO_4)_3$ in $Li_{3-2x}(V_{1-x}Ti_x)_2(PO_4)_3$/C can promote graphitization on particle surfaces. Moreover, the blurred phase boundaries observed for $Li_{3-2x}(V_{1-x}Ti_x)_2(PO_4)_3$/C ($x = 0.025$) cannot be seen in the non-doped and the other Ti-doped $Li_3V_2(PO_4)_3$/C samples. In this study, we could not make sure the stabilization happened in the sample with $x = 0.025$ at room temperature clearly. This phenomenon implies that doping of another transition metal to $Li_3V_2(PO_4)_3$ also has a potential to change the composition of crystalline phase boundary. Therefore, crystalline phases of $x = 0.025$, which are not identified at present, may be the cause of deterioration in the charge-discharge performance.

3.3 Electrochemical Properties of $LiFePO_4$ Cathode Materials Coated with Newly Developed Carbon Black

All the carbon-coated $LiFePO_4$ samples were confirmed from the XRD patterns to crystallize in an olivine type structure. The elemental analysis clarified that the amounts of carbon contained in $LiFePO_4$ synthesized with CB1 or AB are 6.82 and 7.08 wt%, respectively, whereas in the sample with PS the amount 2.86 wt%. Moreover, in $LiFePO_4$ carbon-coated with both CB1 and PS, the carbon amount was evaluated to be 7.44 wt%. It was suggested that in the sample carbon-coated with both CB1 and PS, the carbon derived from PS is very few, since the carbon amount of $LiFePO_4$ with both CB1 and PS is similar to that of the samples with CB1 or AB. These results suggest that the existence of CB1 prevents the deposition of carbon layer. In the calcination process, most of added polystyrene vaporize, and a small portion of polystyrene can be converted to carbon materials. CB1 has the characteristics of developed "structure" and high specific surface area. These characteristics imply that CB1 promotes vaporization of polystyrene during calcination. Therefore, the elementary analysis indicates that the amount of carbon deposited on $LiFePO_4$ with CB1 and PS is less than that of $LiFePO_4$ with PS.

To investigate the effects of CB1 on $LiFePO_4$ particle surface morphology and mass proportion, the SEM backscattered electron (BE) images of the cathode electrodes were taken, and the results are shown in Figure 13. In the images, the large white masses correspond to the $LiFePO_4$ particles, and the small grey ones, deposited around $LiFePO_4$, are carbon blacks. The particle size of $LiFePO_4$ coated with CB1, AB, and both CB1 and PS are found to be 0.1-0.7, 0.4-1.0, and 0.03-0.5 μm, respectively. The images represents that CB1 particles are dispersed on $LiFePO_4$ particles but do not cover the particle surfaces uniformly.

(a)

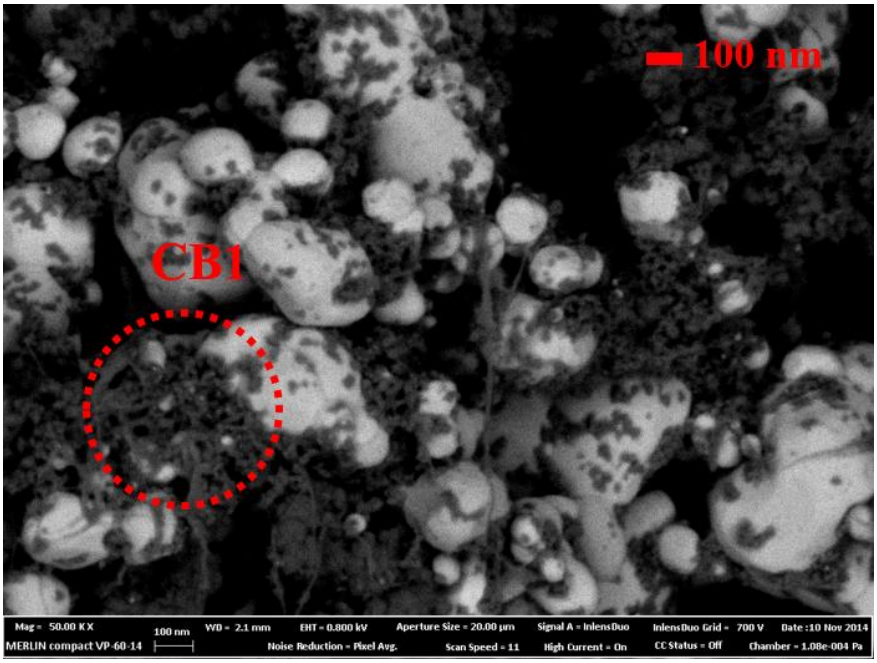
100 nm
CB1
Mag = 50.00 K X
100 nm
WD = 2.1 mm
EHT = 0.800 kV
Aperture Size = 20.00 µm
Signal A = InlensDuo
InlensDuo Grid = 700 V
Date :10 Nov 2014
MERLIN compact VP-60-14
Noise Reduction = Pixel Avg.
Scan Speed = 11
High Current = On
CC Status = Off
Chamber = 1.08e-004 Pa

(b)

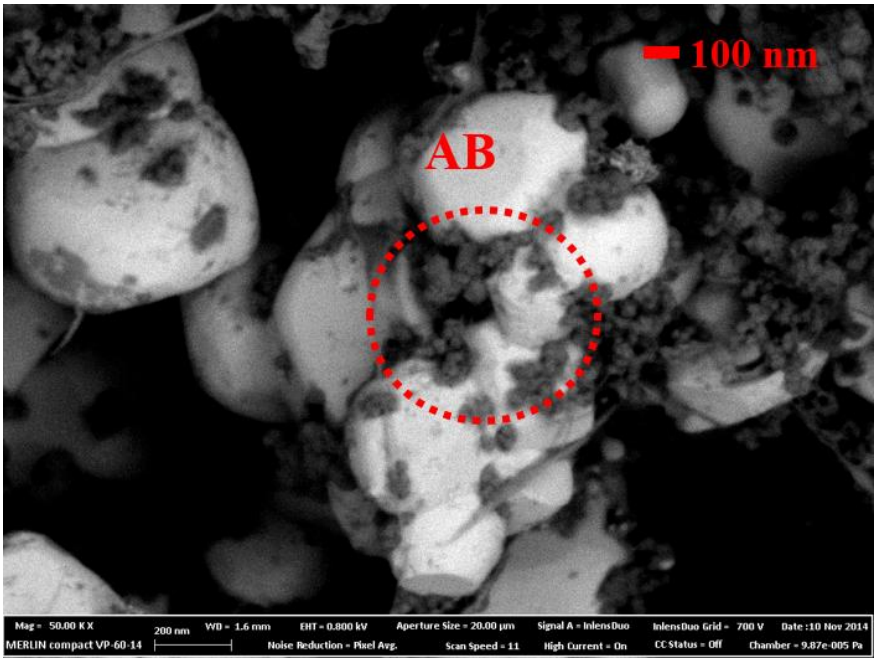
100 nm
AB
Mag = 50.00 K X
200 nm
WD = 1.6 mm
EHT = 0.800 kV
Aperture Size = 20.00 µm
Signal A = InlensDuo
InlensDuo Grid = 700 V
Date :10 Nov 2014
MERLIN compact VP-60-14
Noise Reduction = Pixel Avg.
Scan Speed = 11
High Current = On
CC Status = Off
Chamber = 9.87e-005 Pa

(c)

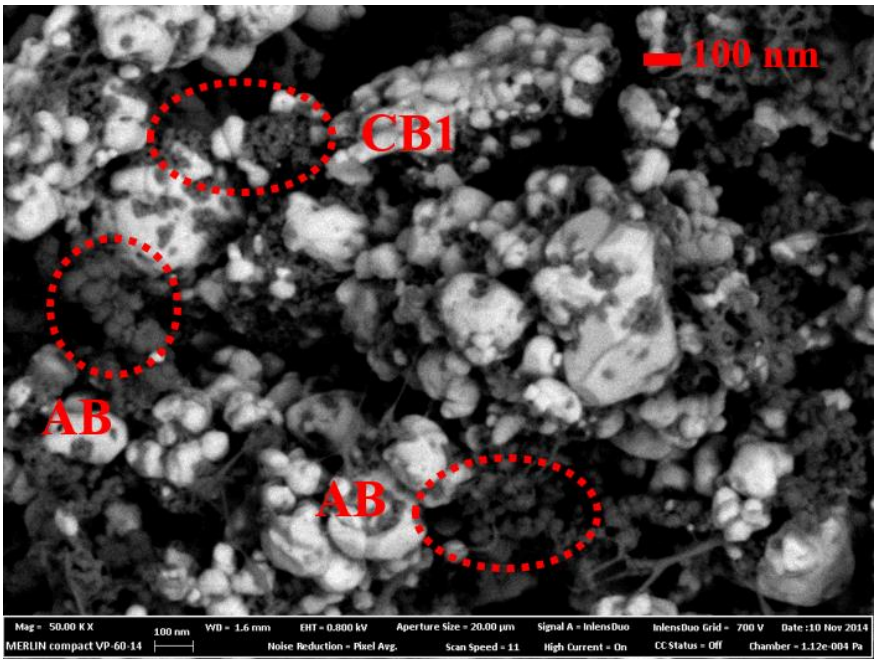

Figure 13. Compositional images in backscattered electron mode of cathode electrodes of the $LiFePO_4$ samples carbon-coated with (a) CB1, (b) AB, and (c) both CB1 and PS.

Moreover, to clarify the particle morphology and the conditions of carbon existing on the samples surface, we performed the TEM observation of the carbon-coated $LiFePO_4$ samples, and the obtained results are given in Figure 14. For the $LiFePO_4$ samples coated with CB1 or AB, the carbon layers deposited on the $LiFePO_4$ surface are hardly seen, whereas for $LiFePO_4$ coated with both CB1 and PS, those derived from PS are observed clearly like the sample coated with PS. The sample with CB1 indicated that CB1 inhibited particle growth. Compared with the case of CB1, the carbon layers derived from PS inhibited $LiFePO_4$ particles growth more efficiently during calcination. Similarly, the two-step carbon-coating method with CB1 and PS should produce fine $LiFePO_4$ particles. This finding suggests that particle growth effect of carbon coating process is more clearly dependent on the existence of carbon layers derived from PS not the existence of CB1. These figures imply that AB cannot inhibit particle growth of $LiFePO_4$ during calcination.

The thickness of the electrodes of samples with AB, CB1, PS, and CB1 and PS were 15.5, 12.1, 15.6, and 10.8 μm, respectively. The density of the electrodes of samples with AB, CB1, PS, and CB1 and PS were 1.6, 2.1, 1.9, and 2.8 g cm^{-3}, respectively. The electrode densities are reflected by the $LiFePO_4$ particle sizes. In Figure 14, the large particles such as $LiFePO_4$ with AB tend to have large interspace between particles, therefore leading to the deterioration of electrode density. TEM observation indicates that the particle size of $LiFePO_4$ with PS is slightly larger than $LiFePO_4$ with CB1 and PS. Nevertheless, the electrodes density of $LiFePO_4$ with PS is significantly lower than $LiFePO_4$ with CB1 and PS. This result means that the actual particle mean size of $LiFePO_4$ with PS is considerably larger than $LiFePO_4$ with CB1 and PS. During the high temperature calcination, the particles of $LiFePO_4$ with PS may aggregate and become formed into secondary particles. In fact, the electrode density of $LiFePO_4$ with PS is in the same range as those of the samples of $LiFePO_4$ with AB or CB1.

(a)

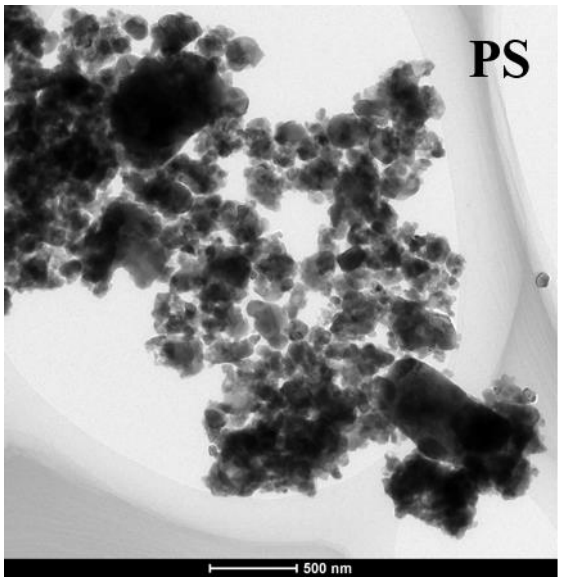

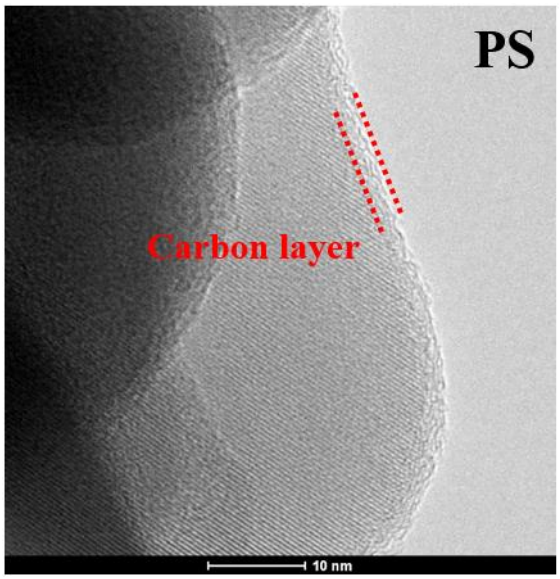

(b)

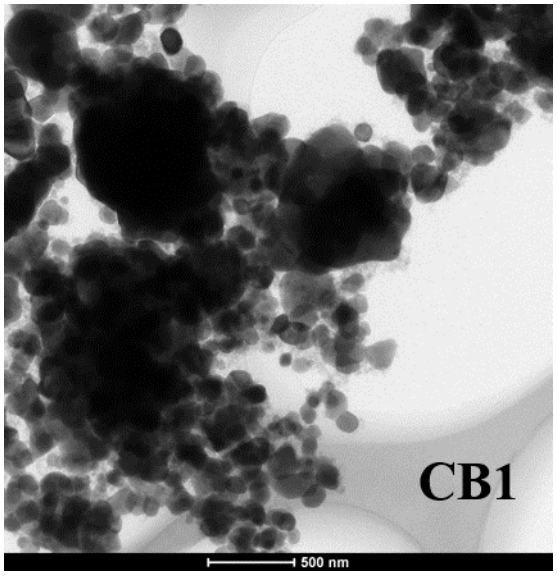

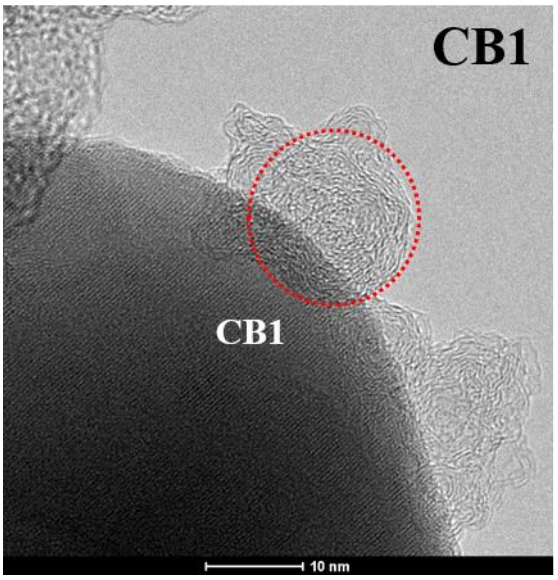

(c)

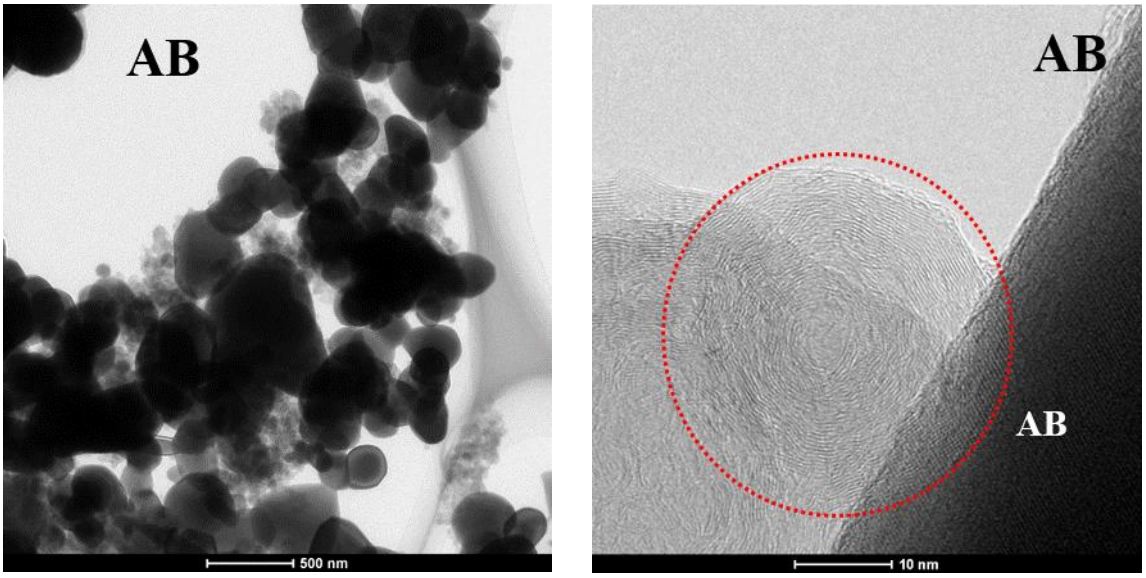

(d)

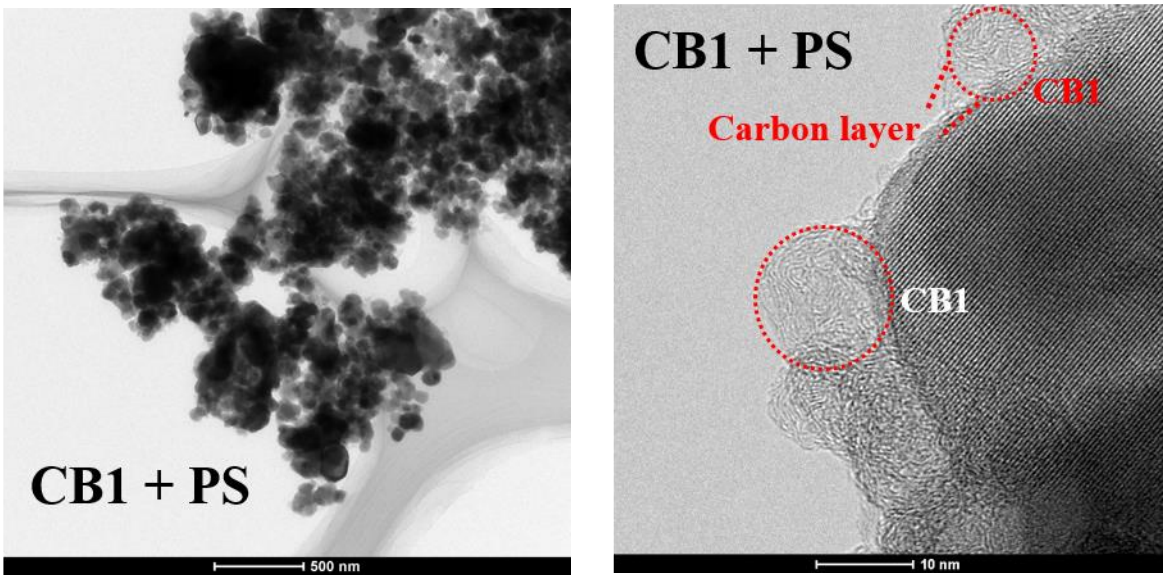

Figure 14. HRTEM images of the $LiFePO_4$ samples carbon-coated with (a) PS, (b) CB1, (c) AB, and (d) both CB1 and PS.

The rate performances of the carbon-coated $LiFePO_4$ samples are represented in Figure 15. The charge and discharge measurements of carbon-coated $LiFePO_4$ with CB1, AB, and PS were conducted from 0.5C to 20C in continuous cycling. Compared with the sample with AB, the discharge capacity of $LiFePO_4$ carbon-coated with CB1 is considerably high. Moreover, the sample with both CB1 and PS exhibits the extremely efficient discharge capacity among the present samples. As compared with $LiFePO_4$ coated with PS, $LiFePO_4$ carbon-coated by two steps with CB1 and PS is found to achieve the high charge-discharge capacity even at high C rates.[4,5] From this result, $LiFePO_4$ with CB1 and AB samples which are not covered with carbon layers indicate a deteriorating discharge capacity at low current densities. Moreover, at high current densities, $LiFePO_4$ coated with PS which are covered with carbon layers shows a remarkable decrease in discharge capacity. Hence, especially at low current densities, $LiFePO_4$ should be covered with carbon layers on the surfaces. In addition, the charge-discharge measurements of $LiFePO_4$ with PS exhibit that the particles covered with only carbon layer cannot maintain sufficient electronic conductivity at high current densities.

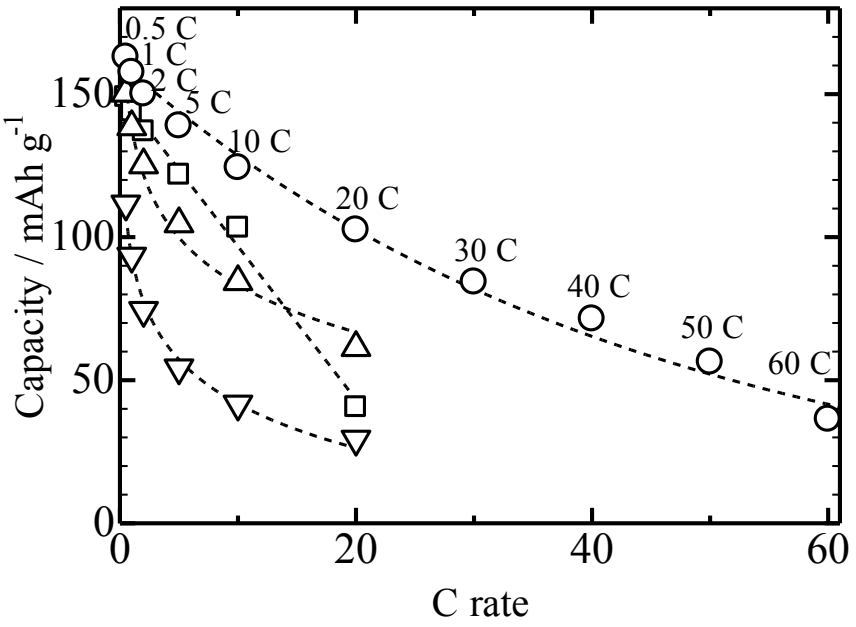

Figure 15. Discharge capacity of carbon coated $LiFePO_4$ at 5th cycles for various rates; (△) CB1; (▽) AB; (□) PS; and (○) CB1 and PS.

The results of the cycle performances are illustrated in Figure 16. The discharge capacity of $LiFePO_4$ carbon-coated with both CB1 and PS goes up to over 100 mAh g^{-1} at 20C, and furthermore, 40 mAh g^{-1} at 60C. The samples of $LiFePO_4$ carbon-coated with both CB1 and PS exhibit the discharge capacity close to the theoretical capacity at low current densities. These results mean that CB1 behaves well as conductive materials between $LiFePO_4$ particles and compensates for the lack of electronic conductivity. In other words, the networks of electronic conduction cannot maintain adequately by usage of only AB for the manufacture of the electrodes. At high current densities, the decrease in discharge capacity were observed for samples with low electrode density. On the other hands, the decrease in discharge capacity is less significant in the samples of $LiFePO_4$ with CB1 and PS than in the samples of $LiFePO_4$ with CB1, AB or PS. From this aspect, active materials should be covered with carbon layers for maintaining high performance at low current densities. At high current densities, the capacity deterioration is not dependent on the presence or absence of carbon layers derived from polystyrene on particles, although active materials should be fine particles for keeping continuous charge-discharge reactions. Microparticulation of active materials is important to make to particle-to-particle contacts and to increase electronic paths.

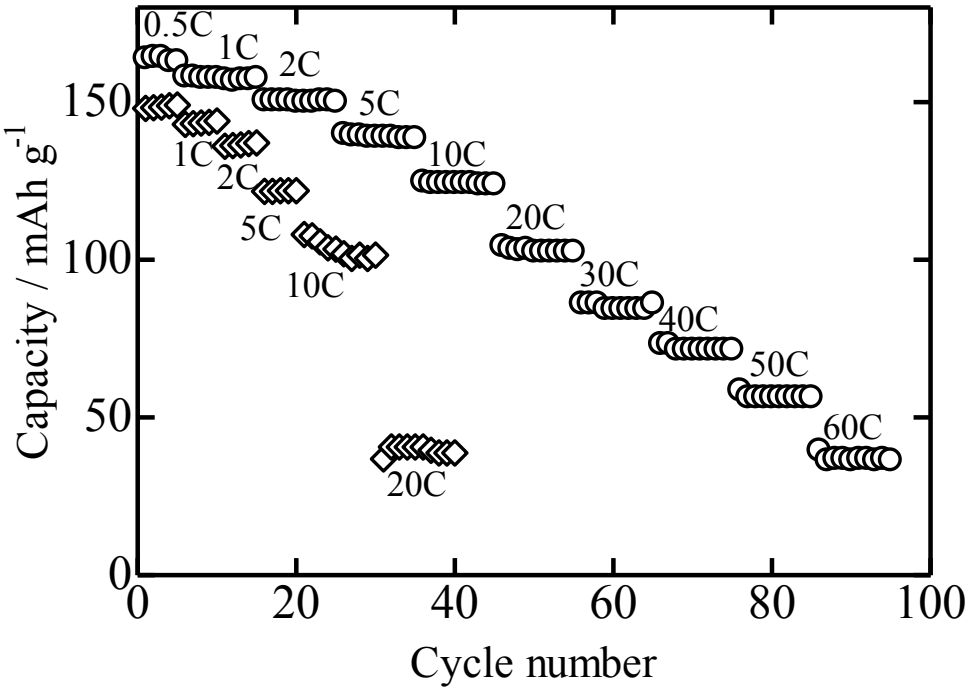

Figure 16. Cycle performances of $LiFePO_4$ carbon-coated with (◇) PS and (○) both CB1 and PS from 0.5 to 60C.

4. Conclusions

4.1 Summary and conclusions on Electrochemical Properties of $Na_3V_2(PO_4)_3$/C Composites Synthesized by Solid Phase Process

It is confirmed that the surface of 700-NVP/C is covered with uniform carbon layers, which provide excellent electrochemical performances. In the meantime, the surface of 600-NVP is covered with poor carbon coating layers, resulting in inferior charge-discharge performances. Moreover, in 800-NVP/C and 900-NVP/C, generated carbon materials are not only deposited on particle surfaces but also aggregated around particles as smoke-like carbon materials. In terms of a $NaVP_2O_7$ impurity phase, calculations by Rietveld refinement reveal that 800-NVP/C and 900-NVP/C have higher proportions of $NaVP_2O_7$ than 600-NVP/C and 700-NVP/C. 700-NVP/C has the lowest $NaVP_2O_7$ proportion. Hence, deterioration of discharge performance observed for 600-NVP/C cannot be regard with the existence of $NaVP_2O_7$. This outcome suggests that the formation of carbon layers on NVP particles inhibits the production of $NaVP_2O_7$. The carbon coating method can achieve the improvement in electronic conductivity on NVP particle surfaces and the inhibition of impurity phase production at the same time. Therefore, this method is the promising means to improve electrochemical properties of NVP.

4.2 Summary and conclusions on Improvement of High Rate Performances for Ti-Doped $Li_3V_2(PO_4)_3$ Cathode Materials

From the temperature dependent conductivity measurements for $Li_3V_2(PO_4)_3$ without carbon-coating, the phase transition from α- to γ-phase at room temperature occurs assisted by substituting Ti for V sites. XRD patterns and the conductivity measurements imply that the stabilization of the γ-phase is completed at the substitution ratios over $x = 0.10$. The discharge capacities of the samples with over $x = 0.050$ are improved greatly at 60C. This is due to the improvement in Li ion conductivity of the stabilized γ-phase at room temperature. The laminate structure of graphitic layers is hardly seen on the particle surfaces of the sample with $x = 0.025$.

In contrast, the clear phase boundaries between $Li_3Ti_2(PO_4)_3$ and $Li_3V_2(PO_4)_3$ phases and the existence of the graphitic carbon layers on the particle surfaces of $Li_{3-2x}(V_{1-x}Ti_x)_2(PO_4)_3$/C are seen over $x = 0.10$. This means that the crystallization of $Li_3Ti_2(PO_4)_3$ in $Li_{3-2x}(V_{1-x}Ti_x)_2(PO_4)_3$/C can promote graphitization on the particle surface. In conclusion, the improvement of electrochemical properties of Ti-doped $Li_3V_2(PO_4)_3$ is promoted not only by stabilization of the γ-phase but also by the graphitization on $Li_3V_2(PO_4)_3$ particle surfaces.

4.3 Summary and conclusions on Electrochemical Properties of $LiFePO_4$ Cathode Materials Coated with Newly Developed Carbon Black

A much more improvement in electrochemical performance is observed in the $LiFePO_4$ carbon-coated with both CB1 and PS, compared with the sample with CB1. Such results suggest that size-reduced $LiFePO_4$ particles contribute to further internal diffusion of Li^+ and consequently improve its electrochemical properties. Moreover, for the sample with PS, a small amount of carbon layers derived from PS play important roles in the improvement of the charge-discharge performance. In addition, for the sample with both CB1 and PS, CB1 can greatly enhance electronic conductivity on $LiFePO_4$ particle surfaces covered with carbon layers, and can produce conductive paths in the electrode.

The electrode density of $LiFePO_4$ with PS is significantly lower than that of $LiFePO_4$ with both CB1 and PS. Thus, this result imply the possibility that the particles of $LiFePO_4$ with PS are generated as secondary particles during synthesis process. The charge-discharge measurements for $LiFePO_4$ coated with PS exhibit insufficient electronic conductivity at high current densities. The deterioration of discharge capacity is observed for $LiFePO_4$ with CB1, AB, and PS at high current densities. However, $LiFePO_4$ with both CB1 and PS exhibit excellent discharge performances at high current densities. On the issue of the charge-discharge measurements, active materials should be fine particles for keeping continuous charge-discharge reactions at high current densities.

5. General Conclusions

In this study, the carbon coating method by adding polystyrene to the precursor of cathode materials is verified to be an excellent method to produce oxoacid cathode materials that exhibit not only high electronic conductivity on the surfaces of active particles but also improvement in ionic diffusion of ions in the electrodes, providing an realistic usage in secondary batteries. The oxoacid active materials synthesized by this carbon coating method show no sign for reduction in oxidation states of transition metal. Therefore, this carbon coating method is expected to be used in near future battery technology.

Reference

1. Y.-D. Cho, G. T.-K. Fey, and H.-M. Kao, *J. Power sources*, 18**9**, 252-262 (2009)
2. B. Kang, and G. Ceder, *Nature*, **458** 190-193 (2009)
3. X. Zhi, G. Liang, L.Xang, X. Ou, L. Gao, and X. Jie, *J. Alloy. Compud*., **503**, 370-374 (2010)
4. M. Konarova and I. Taniguchi, *J. Power Sources*, **195**, 3661-3667 (2010).
5. Y. Long, Y. Shu, X. Ma, and M. Ye, *Electrochim. Acta*, **117**, 105-112 (2014).
6. A. K. Padhi, K. S. Nanjundaswamy, C. Masquelier, and J. B. Goodenough, *J. Electrochem. Soc.*, **144**, 2581-2586 (1997)
7. B. L. Cushing, and J. B. Goodenough, *J. Solid State Chem.*, **162**, 176-181 (2001)
8. J. Gaubicher, C. Wurn, G. Goward, C. Masquelier, and L. Nazer, *Chem. Mater.*, **12**, 3240-3242 (2000)
9. C. Masquelier, C. Wurm, J. Rodríguez-Carvajal, J.Gaubincher, and L. Nazer, *Chem. Mater.*, **12**, 525-532 (2000)
10. P. Barpanda, G. Liu, C. D. Ling, M. Tamaru, M. Avdeev, S.-C. Chung, Y. Yamada, and A. Yamada, *Chem. Mater.*, **25**, 3480-3487 (2013)
11. J.-N. Chotard, G. Rousse. R. David, O. Mentré, M. Courty, and C. Masquelier, *Chem. Mater.*, **27**, 5982-5987 (2015)
12. H. Huang, S.-C. Yin, T. Kerr, N. Tayler, and L. F. Nazer, *Adv. Mater.*, **14**, 1525-1528 (2002)
13. L. S. Plashnitsa, E. Kobayashi, Y, Noguchi, S, Okada, and J. Yamaki, *J. Electrochem. Soc.*, **157**, A536-A543 (2010)
14. M. Y. Saïdi, L. Barker. H.Huang. J. L. Swoyer, and G. Adamson, *J. Electrochem. Soc. Solid State let*., **5**, A149-A151 (2002)
15. X. Du, W. He, X. Zhang, Y. Yue, H. Liu, X. Zhang, D. Min, X. Ge, and Y. Du, J. *Mater. Chem.*, **22** 5960-5969 (2012)
16. S.-W. Kim D.-H Seo, X. Ma, G. Ceder, and K. Kang, *Adv. Energy Mater.*, **2**, 710-721 (2012)
17. M. D. Slater, D. Kim, E. Lee, and C. S. Johnson, *Adv. Funct. Mater*., **23**, 947-958 (2013)

18. S. Li, Y. Dong, L. Xi, X. Xu, L. He, and L. Mai, *Adv. Mater.*, **26**, 3545-3553 (2014)

19. S.-C. Yin, P. S. Strobel, H. Grondey, and L. F. Nazer, *Chem. Mater.*, **16**, 1456-1465 (2004)

20. L. Si, Z. Yuan, L. Hu, Y. Zu, and Y. Qian, *J. Power sources*, **272**, 880-885 (2014)

21. W. Song, Z. Wu, J. Chen, Q. Lan, Y. Zhu, Y. Yang, C. Pan, H. Hou, M. Jing, and X. Ji, *Electrochim. Acta*, **146**, 142-150 (2014)

22. S. C. Yin, H. Grondey, P. Strobel, H. Huang, and L. F. Nazar, *J. Am. Chem. Soc.*, **125**, 326-327 (2003).

23. D.-W. Han, S.-J. Lim, Y.-I. Kim, S. H. Kang, Y. C. Lee, and Y.-M. Kang, *Chem. Mater.*, **26**, 3644-3650 (2014).

24. C. Deng, S. Zhang, S. Y. Yang, Y. Gao, B. Wu, L. Ma, B. L. Fu, Q. Wu, and F. L. Liu, *J. Phys. Chem. C*, **115**, 15048-15056 (2011).

25. M. Sato, H. Ohkawa, K, Yoshida, M.Saito, K. Uematsu, and K. Toda, *Solid State Ionics*, **135**, 137-142 (2000).

26. T. Suzuki, K. Yoshida, K. Uematsu, T. Kodama, K. Toda, Z.-G. Ye, and M. Sato, *Solid State Ionics*, **104**, 27-33 (1997).

27. T. Suzuki, K. Yoshida, K. Uematsu, T. Kodama, K. Toda, Z.-G. Ye, M. Ohashi, and M. Sato, *Solid State Ionics*, **113-115**, 89-96 (1998).

28. S. Tajimi, Y. Ikeda, K. Uematsu, K. Toda and M. Sato, *Solid State Ionics*, **175**, 287-290 (2004).

29. K. Uematsu, A. Ochiai, K. Toda, and M. Sato, *J. Ceram. Soc. Jpn*, **115**, 450-454 (2007)

30. C. Sato, E. Hoshi, K. Uematsu, T. Ishigaki, K. Toda, and M. Sato, *Trans. Mater. Res. Soc Jpn.*, **35**, 397-400 (2010).

31. M. Sato, K. Uematsu, H.Tsuji, K. Toda, T. Ishigaki, and H. Ohkawa, Japan patent, 5765798

32. A. K. Padhi, K. S. Nanjundaswamy, and J. B. Goodenough, *J. Electrochem. Soc.*, **144**, 1188-1194 (1997).

33. D. Morgan, G. Ceder, M. Y. Saïdi, J. Barker, J. Swoyer, H. Huang, and G. Adamson, *Chem. Mater.*, **14**, 4684-4693 (2002).

34. C. Masquelier, A. K. Padhi, K. S. Nanjundaswamy, and J. B. Goodenough, *J. Solid State*

Chem., **135**, 228-234 (1998)

35. A. Yamada, S. C. Chung, and K. Hinokuma, *J. Electrochem. Soc.*, **148**, A224-A229 (2001).

36. M. Wagemaker, B. L. Ellis, D. Lützenkirchen-Hecht, F. M. Mulder, and L. F. Nazer, *Chem. Mater.*, **20**, 6313-6315 (2008)

37. H. Nakano, K. Dokko, S. Koizumi, H. Tannai, and K, Kanamura, *J. Electrochem. Soc.*, **155**, A909-A914 (2008).

38. R. Dominko, M. Bele, M. Gaberscek, M. Remskar, D. Hanzel, S. Pejovnik, and J. Jamnik, *J. Electrochem Soc*., **152**, A607 (2005).39. F. Izumi, and K. Momma, *Solid State Phenom.*, **130**, 15-20 (2007)

40. J. D. Wilcox, M. M. Doeff, M. Marcinek, and R. Kotecki, *J. Electrochem. Soc.*, **154**, A389-A395 (2007)

41. S. Y. Lim, H. Kim, R. A. Shakoor, J. Jung, and J. W. Choi, *J. Electrochem. Soc.*, **159**, A1393-A1397 (2012)

42. Y. Zhou. Z. Liu, J. Zhang, W. Wang, and Y. Liu, *J. Electrochem. Soc.*, **161**, A968-A973 (2014)

43. X. Pu, W. He, X. Zhang, Y. Yue, H. Liu, X. Zhang, D. Min, X. Ge, and Y. Du, *J. Mater. Chem.*, **22**, 5960-5969 (2012)

44. X. Sun, Y. Xu, M. Jia, D. Ding, Y. Liu, K. Chen, *J. Mater. Chem. A*, **1**, 2501-2507 (2013)

45. C. Wei, W. He, X. Zhang, S. Liu, C. Jin, S. Liu, and Z. Huang, *RSC Adv.*, **5**, 288662-28669 (2015)

46. A. P. Tang, X. Y. Wang, S. Y. Yang, and J. Q. Cao, *J. Appl. Electrochem.*, **38**, 1453 (2008).

47. Y. Xia, W. Zhang, H. Huang, Y. Gan, C. Li, and X. Tao, *Mater. Sci. Eng. B*, **176**,

48. A. Ataiq, M. Menétrier, L. Croguennec, E. Suard, and C, Delmas, *J. Mater. Chem.*, **12**, 2971-2978 (2002)

Acknowledgment

The author would like to express his heartfelt gratitude to Professor Dr. Mineo Sato, Faculty of engineering, Niigata University, for his continuous guidance, his invaluable suggestions, and his science encouragement through this project.

The author would like to thank Professor Dr. Hiroshi Imaizumi, Professor Dr. Takuya Kodama, Associate Professor Dr. Naoki Kano, Associate Professor Dr. Kenji Toda, Associate Professor Dr. Noriyuki Gokon, Research Associate Dr. Atsushi Itadani, Niigata University, for their patient guidance and encouragement.

The author would also like to thank Dr. Kazuyoshi Uematsu, Niigata University, for his helpful suggestions and earnest advice.

Our special thanks are due to Dr. Hideki Hashimoto of Okayama University in the measurement of TEM images.